SLURRY PHASE IRON CATALYSTS FOR INDIRECT COAL LIQUEFACTION

Contract No. DE-FG22-95PC95210

to

The University of New Mexico

7/5/94 - 7/4/98

Fourth Semi-Annual Progress Report

Covering the Period from 1/5/97 - 7/4/97

Prepared for

U. S. Department of Energy
Pittsburgh Energy Technology Center
PETC Project Manager: Richard E. Tischer

Submitted by

Abhaya K. Datye, Professor
Department of Chemical & Nuclear Engineering and
Director, Center for Microengineered Materials
University of New Mexico
Albuquerque, NM 87131

submitted August 8, 1997
revised September 10, 1997

Disclaimer

Abstract

This report describes research conducted to support the DOE program in indirect coal liquefaction. Specifically, we have studied the attrition behavior of iron Fischer-Tropsch catalysts, their interaction with the silica binder and the evolution of iron phases in a synthesis gas conversion process. The results provide signficant insight into factors that should be considered in the design of catalysts for converting coal based syn-gas into liquid fuels.

Table of Contents page

Executive Summary

This report covers the fourth six month period of this three year grant under the University Coal Research program. During this period, we have begun the synthesis of precipitated catalysts using a bench-top spray dryer. The influence of binders on particle strength was also studied using the ultrasonic fragmentation approach to derive particle breaking stress. A similar approach was used to derive particle strength of catalysts obtained from Mr. Robert Gormley at FETC. Over the next six month period, this work will be continued while the catalysts prepared here will be examined by TPR to determine reducibility and the extent of adverse iron-silica interactions.

A fundamental study of Fe/silica interactions has been performed using temperature programmed reaction and TEM to provide understanding of how the silica binders influence the activity of Fe catalysts. To understand differences in the reducibility of the iron phase caused by silica, we have set up a temperature programmed reduction facility. TPR in H_2 as well as in CO was performed of Fe/SiO_2 catalysts prepared by impregnation as well as by precipitation. What is unique about these studies is that high resolution TEM was performed on samples removed from the reactor at various stages of reduction. This helps provide direct evidence for the phase changes that are detected by TPR.

We have continued the analysis of catalysts received from slurry reactor runs at Texas A&M university (TAMU) and the University of Kentucky Center for Applied Energy Research (CAER) by x-ray diffraction. The purpose of the XRD analysis was to determine the phase composition of catalysts derived from a slurry reaction run using Fe Fischer-Tropsch catalysts. We had previously described how catalyst removed in the hot wax may oxidize to magnetite if the wax is air-exposed. We have now received catalysts from CAER that were removed under a protective inert blanket, and we are in the process of analyzing them, but preliminary work presented here shows very little oxide by XRD. However, the catalyst that was used in these runs at CAER was a different composition than that used in previous runs, so the protective effect of an inert blanket will need further study. Finally, we point out how the interference by the wax can make it difficult in some cases to analyze the phases in a Fe catalyst. Several approaches have been used to remove the interference from the wax and we come to the surprising conclusion that α-Fe may be present in a working slurry reactor despite the high CO/H_2 ratio. Further work is underway to corroborate this finding.

Technical Objectives

The objective of this research project is to perform fundamental research in support of catalyst development for slurry phase bubble column reactors for Fischer-Tropsch synthesis. The overall program is divided into the following tasks:

Task 1. Catalyst Particulate Synthesis
Task 2. Catalyst Binder Interactions

In task 1, we will first study factors that determine the attrition resistance of slurry phase Fe catalysts. Fundamental understanding of the attrition phenomenon will be used to guide the synthesis of novel precipitated catalysts that overcome some of the limitations of current

generation catalysts. The investigation of catalyst microstructure as a function of treatment will help determine the optimal treatment protocols for F-T synthesis catalysts. Since the use of binders is considered essential for providing the desired attrition resistance, the second task is to perform fundamental studies of catalyst-binder interactions. These studies will use model catalysts that can be studied by high resolution transmission microscopy to investigate the nature of interfacial phases at the Fe-binder interface. A better understanding of the phenomena that lead to catalyst-binder interactions will help us design improved catalysts for indirect coal liquefaction.

Task 3. Characterization of catalysts received from CAER, Univ. of Kentucky, and from Texas A&M.

Task 3 was not included in our original proposal. However, we are pursuing these studies to help understand catalyst deactivation under actual reaction conditions.

Technical Progress
(Please note that Task 2 is being described before Task 1, for this report only)

Task 2 - Catalyst-binder interaction

Overview

We have studied catalyst-binder interactions by using temperature programmed reduction of supported and unsupported catalysts to study how the binder-catalyst interaction affects the reducibility of the iron phase.

Experimental

Two silica sphere supported iron catalysts, YJ/1-65A(20 wt % Fe, with 1 wt % Cu) and YJ/1-67(10 wt % Fe), were prepared by conventional incipient wetness impregnation and precipitation respectively. A UCI unsupported catalyst (1185-149, $Fe_2O_3/CuO/K_2O = 88.95/11/0.05$) was used as a reference. In this study, a 10% CO/He or 10% H_2/Ar reductant stream was used with 20-30 mg catalyst sample contained in a U-shaped quartz reactor. A Thermal Conductivity Detector (TCD) was used for the analysis. An in-line CO_2 trap or H_2O trap located between the reactor and the detector was used to remove CO_2 or H_2O formed during TPR process. The sample temperature was ramped in each experiment at 10°C /min to 500°C and then held at the latter temperature for 0.5-1 hour. Following the TPR run, the sample was reoxidized at 500 °C and a second TPR was performed.

For identification of the various phases present during the TPR run we examined samples removed from the reactor using transmission electron microscopy. The precise time where a sample was withdrawn has been indicated on the TPR plots. These TEM images show the morphological transformations that accompany reduction and provide better understanding of the role of the support in Fe F-T catalysts.

Results

The results of CO TPR for the base UCI catalyst are shown in Fig. 1. Precalcination has appreciable effects on the TPR profile of unsupported UCI-1185-149, with the peak representing reduction of hematite to magnetite shifting to higher temperature with increasing calcination temperature. The higher precalcination temperature could cause agglomeration of the catalyst particles and pore structure collapse. It is also possible that the copper oxide phase which is well dispersed in the catalyst as-prepared may segregate into larger particles and hence not be able to facilitate the reduction of hematite to magnetite, as it does in the as-prepared catalyst.

Our preliminary peak assignment is as follows: the first peak represents the reduction of CuO to Cu as confirmed by a similar reduction peak for a copper oxide on silica catalyst. The second peak represents transformation of Fe_2O_3 to Fe_3O_4, while the massive higher temperature peak corresponds to conversion of Fe_3O_4 to α-Fe. These assignments are confirmed by the TEM images shown in Figs 3-6 and the x-ray diffraction pattern in Fig. 7.

Fig. 2 shows a comparison of the 1st and 2nd TPR runs on the UCI base catalyst. The shift in peak temperature suggests that the catalyst has sintered, and this is confirmed by the TEM images. The sharp peak at low temperature in the 1st run TPR is replaced by a much smaller, broad peak in the second run. More important, the 2nd peak (hematite --> magnetite) occurs about 100 °C higher in the 2nd TPR. Comparison of TEM images in Fig. 3 and 5 provide evidence for the underlying phenomena. The magnetite in Fig. 3 is fine grained and with an open pore structure while that in Fig. 5 is much more dense. The reason the magnetite has changed its morphology is that the 1st run TPR causes a sintering of the metallic Fe to large particles as seen in Fig. 4. Since the sample is exposed to air during transfer to the electron microscope, we build up a surface oxide, but otherwise, the sample contains predominantly α-Fe.

The presence of α-Fe in a catalyst that has been reduced in CO at 500 °C is somewhat surprising. We have confirmed the presence of α-Fe via x-ray diffraction. It is possible that the rapid rate of heating does not allow the large Fe particles that are present in the unsupported catalyst to transform into iron carbide. Indeed, as we show in Figs. 8-11, the supported iron catalyst transforms completely to iron carbide under these conditions. Therefore, we conclude that particle size plays a major role in influencing the transformation of the iron oxide to iron carbide over the time scale of the TPR experiment. The formation of surface carbonaceous materials seems to go hand in hand with the formation of iron carbide. No carbonaceous species are seen in Fig. 4 in contrast to Fig. 10 which comes from the supported catalyst but after treatment at identical conditions.

After the second TPR run, the sample was again imaged in the TEM (Fig. 6). We find that large α-Fe particles are present but there is a significant amount of unreduced magnetite present as well. From the TPR plot, we infer that the reduction of magnetite --> α-Fe is not complete in the 2nd TPR. This could again be a result of the segregation of Cu during the redox cycle and sintering of the catalyst. An x-ray diffraction pattern of this catalyst after the 2nd TPR is shown in Fig. 7. This pattern was obtained by treating a larger amount of catalyst (0.120 g) instead of the usual (0.020 g). The larger amount of catalyst may further diminish

the extent of reduction, but overall the pattern is consistent with the TEM image in Fig. 6. Essentially, the major peaks are α-Fe (44.7 °, 65 ° and 82.3 °), a small Cu peak (43.2 °) with the remainder being magnetite peaks. The 100% peaks of magnetite and a-Fe are of equal intensity. The XRD pattern therefore confirms that reduction in CO transforms the magnetite to α-Fe.

The role of the silica support on the reducibility of the Fe phase is shown in Figs 8-11. Fig. 8, the TPR plot shows that calcination at temperatures up to 430 °C has a negligible effect on the TPR profiles. This catalyst only contains a small amount of Cu so a distinct Cu peak cannot be seen in the TPR plot. In view of the small amount of iron in this catalyst, it is not surprising that the peak for hematite --> magnetite is only a small blip. Hence, the first major peak represents the reduction of the iron phase. Samples were removed for TEM after 380 °C (Fig. 9) and after 500 °C reduction (Fig. 10) as indicated by the arrows in Fig. 8. The TEM image and the electron diffraction patterns confirm that the sample has transformed into iron carbide by 380 °C. The only major change from 380 °C to 500 °C is the deposition of graphitic carbon and this must account for the consumption of CO over this temperature range. The presence of the carbide phase appears to be necessary before the Boudouard reaction deposits significant amounts of carbonaceous species on the catalyst surface.

Future Work

We plan to use the TPR technique to quantify the reducibility of the catalysts we prepare via spray drying (task 1) and to understand the role of the silica support in modifying catalyst behavior.

Task 1: Catalyst Particulate Synthesis

Overview

In the previous six-monthly report, we showed how ultrasonic excitation followed by sedigraph particle size distribution provides a simple test to determine the strength of catalyst agglomerates. Using this method, we have examined the particle strength of several catalyst formulations synthesized at FETC by Mr. Robert Gormley (Figs. 12-14) . During this period, we have also brought on line a bench-top spray dryer that was used to prepare various catalyst formulations, with and without binder. The strength of the spray dried particles and their morphology was investigated using ultrasonic fragmentation and scanning electron microscopy, respectively. Initial results are presented in Figs. 15-16. The results suggest that addition of precipitated silica and spray drying yields powder agglomerates that are considerably stronger than the unsupported hematite catalyst. During this period we have also continued our studies of attrition testing methods and present a comparison of the ultrasonic fragmentation and uniaxial compaction approaches in Figs. 17-18.

Ultrasonic Fragmentation tests

Experimental details for the ultrasonic fragmentation approach have been described in detail in our previous reports. We disperse 1 g of catalyst in 50 ml of deionized water. A Sedigraph particle size analyzer is used to determine the size distribution. The suspension is then sub-

jected to ultrasonic energy using a Tekmar high intensity probe. After different extents of ultrasonic irradiation, the particle size distribution is analyzed to detect the mode of particle fragmentation. The method can also be used to derive a quantitative measure of agglomerate strength as explained previously in our progress reports.

We have used the ultrasonic fragmentation approach to study the agglomerate strength of several catalysts prepared by Mr. Robert Gormley at FETC. Fig. 12 shows the fragmentation results of three precipitated Cu-promoted Fe catalysts, which had alumina added in different ways. Two of the samples, 112 and 117 had K added, and were calcined at 350 °C in air. The results in Fig. 12 suggest that calcination does not appear to significantly improve the strength of the agglomerates, at least as seen by the ultrasonic fragmentation approach.

Fig. 13 shows fragmentation results for catalysts, without alumina and with co-precipitated alumina. Comparison of the two catalysts show that addition of alumina does not impart significant additional strength, at least as seen in these tests. As shown in Fig. 14, the powders used here are not spray dried. They have irregular morphologies and the drying method used appears to provide agglomerates that are quite strong as prepared. Hence the added alumina or the calcination step does not seem to lead to any further strengthening. Further tests need to be performed after these catalysts have been activated and used for F-T synthesis to see if the calcination or alumina addition result in strength improvements.

Catalyst Synthesis via Spray Drying

During the last six month period, we brought on line a Bucchi spray dryer which we have used to prepare spray dried catalysts with differing amounts of binder. These catalysts were prepared with and without a calcination step, with calcination temperatures up to 600 °C being used. The base catalyst was prepared at FETC with the kind assistance of Mr. Robert Gormley and his associates.

Sample Number: PRFECUK-ED19-98. **Description**: Precipitated Fe, Cu, K, washed to remove nitrate, then mixed with 813 ml water **Wt% Metals**: 64.80% Fe, 6.24% Cu, 0.01% K by ICP based on dried wt.

One hundred milliliters of the wet form of PRFECUK-ED19-98 was ultrasonicated at an amplitude of 20 for 2 min to break up any loose agglomerates. The sample was then mixed with 11 ml of sodium silicate solution (N brand from PQ Corp.). Dilute Nitric acid (0.1 N) was added dropwise while the slurry was stirred until the pH was about 7. The mixture was stirred for a further 20 minutes and then filtered using a Buchner funnel. It was then washed at least twice with deionized water to get rid of the Na^+ ions. Deionized water was then added to prepare 250 ml of slurry. A Buchi 190 Mini Spray Dryer was then used to spray-dry the slurry. The powder was collected in a cyclone trap. The inlet temperature of the spray drier was 200 °C with the outlet being maintained over 100 °C.

Fig. 15 shows an SEM image of the spray dried powder. Spherical particles can be seen with a particle size distribution that is typical for a spray dried powder. These particles are smaller than those desired for a commercial F-T process, however they represent the best we could achieve with our bench-top spray dryer. Ultrasonic fragmentation analysis of this powder

was performed using conditions similar to those used previously and the results are shown in Fig. 16. We can see that the powders show erosion as the primary breakdown mechanism with fine particles starting to appear after 5 min of ultrasound application.

For comparison, we present in Fig. 17 ultrasonic fragmentation results on two of the base catalysts we had reported in our Feb. 97 report. One of these is a precipitated Fe catalysts used in Laporte I (had 11.3 wt% silica and was not sieved to remove fines) and the other is a Vista alumina powder. It is evident that the Vista alumina powder shows minimal erosion after 15 minutes of irradiation whereas the base Fe catalyst had disintegrated completely. We can conclude that the spray dried catalyst prepared at UNM (Fig. 15-16) shows considerable improvement over the base catalyst.

Uniaxial Compression Testing

Uniaxial compression testing is a technique for characterizing the strengths of powders and granular materials. A detailed discussion of this method was presented in our Feb 97 report. Uniaxial compression testing has been used by a group at Sandia National Laboratories (SNL) in the study of ceramic granule strength. In this method, the relative density of the compacted sample is plotted vs. the log of the compaction pressure as shown below.

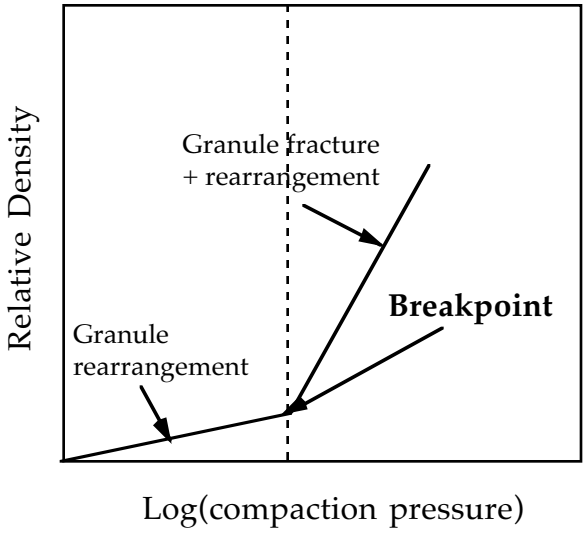

As shown in this plot, compaction data tend to exhibit linear regimes that can be attributed to different compaction mechanisms (2). The breakpoint has been used as a semi-quantitative indicator of powder/granule strength or yield point, and is thought of as the average strength. Recent work at SNL, however, has demonstrated that it is more representative of the lower end of the range of powder or granule strengths.

In our work, we have explored the use of uniaxial compression testing to measure the strengths of Fischer-Tropsch catalysts. An Instron 5565 machine was used for compaction tests of these catalysts. This machine allows different-size dies to be used depending on the amount of

samples available. We have chosen to work with an 1/8" die to minimize the amount of sample required for a given test. In our Feb 97 report, we commented on the sensitivity of the breakpoint determination to how many data points are included in determining the slope of the two linear regimes. Hence we have explored alternative methods to derive the breaking strength.

Experimental Details

Ten milligrams of a powder sample were loaded into the cell of a die with a 1/8" opening. A plunger was then placed on top of the filled die, taking great care not to compress the sample. To account for the error due to deformation of the top plunger and to the compliance of the crosshead, the displacement of the empty fixture as a function of load was subtracted from the displacement of the filled die. Compression tests were conducted by placing the filled die underneath the crosshead of the Instron machine. The crosshead was manually lowered such that it was just touching the top plunger. The displacement gauge was zeroed, and the crosshead was then activated at a rate of 1.00 mm/min. Testing was continued until a load of 1000 N was reached. The sample was repeated for reproducibility.

Results

Fig. 18 shows compaction data for a Davisil silica gel and the two base catalysts shown in Fig. 17. The data are presented in the form of a plot of ln (P) vs. natural strain, e, for a sample of Davisil Silica gel. Similar plots are presented in Fig. 18b for base Fe catalyst UCI-LAPI-COMP-DRUMC (the catalyst used for LaPorte I), and Fig. 18c for VISTA-B-965-500C (alumina support from Vista). The results were analyzed using a model presented by Adams, *et. al.* (1). which yields a value for the breaking strength (sigma) of the particles within the powder sample. According to these plots, Davisil Silica was strongest among the three samples. However, the strengths of the base Fe catalyst and VISTA alumina were not significantly different. Both strengths differed by about 1.2 MPa. In contrast, the ultrasonic fragmentation method showed major differences between these two samples (see Fig. 17). The base Fe catalyst was much weaker than the VISTA catalyst and suffered particle breakup as well as erosion.

Future Work

Although the uniaxial compaction method is simpler to use and requires a small sample size, it does not appear to differentiate very well between samples such as the base Fe catalyst and the alumina support which appear quite different in strength by the ultrasonic fragmentation approach. The important question is how well either of these methods predict catalyst behavior in a slurry reactor, and this will be the subject of our future research over the next year. Our work will involve the synthesis of spray dried Fischer-Tropsch catalysts and an evaluation of their performance in F-T slurry reactor conditions as well as the study of adverse metal-support interactions in these catalysts.

Task-3: Characterization of catalysts from Univ. of Kentucky & Texas A&M

Overview

In our Feb 97 progress report we presented the analysis of samples obtained from Texas A&M university that had been used for over 400 hours in an FT synthesis reactor (run SB-3425). We found that there was no apparent transformation of the carbide into magnetite over the course of this run even though the CO conversion was 80%. While this sample exhibited several peaks that occur in the region where iron carbide diffraction occurs (2.271 Å - 2.108 Å) (see Fig. 11) along with a peak corresponding to α-Fe (2.03 Å)., we wanted to rule out any interference from the wax that the catalyst is embedded in. We therefore present further analysis of this sample that comes to the surprising conclusion that the peaks in the range 2.271 Å - 2.108 Å come from the wax and do not represent iron carbide. After removal of the wax, we find α-Fe to be the major constituent of this catalyst.

A similar XRD analysis of a run from CAER was also performed (run RJO-189). Here we again found no evidence for interconversion of carbide into magnetite over the 3547 hours that the run was performed. However, magnetite was a major constituent of this catalyst as received in the wax. We suspected that while the wax may help protect the sample from oxidation at room temperature, removal of the hot wax in air could cause oxidation of the catalyst. This appeared to be a major difference between the way the catalyst was removed for run RJO-189 (removal in air) and run SB-3425 at Texas A&M (removal under inert). CAER has now provided us with samples from a new run (RJO-236) where the catalyst containing hot wax was removed under an inert blanket. Our analysis, presented here in Figs. 23-24 shows this catalyst contains no iron oxide. Unfortunately, the composition of the catalyst used for runs RJO-189 and RJO-236 was different, and this may account, in part, for the different relative amounts of magnetite and carbide we find by XRD. We hope to receive in the future samples from CAER from a run similar to RJO-189 so that the role of an inert blanket in protecting samples from oxidation can be conclusively established.

Results

XRD analysis of samples in wax from run SB-3425 performed at Texas A&M

Fig. 19 shows an XRD powder pattern of the sample as received from Texas A&M run SB-3425 time on stream = 233 hours (labeled slurry in Fig. 19). Also shown in Fig. 19 is the same sample after soxhlet extraction. It can be seen that the XRD pattern has changed considerably. The α-Fe peak at 2.028 Å is missing and instead we see broad magnetite peaks. The remaining peaks between 40 and 45 ° 2-Theta must be carbide peaks. Also shown in Fig. 19 is the wax as it was stripped off from this catalyst. Comparing the wax XRD pattern with that from the slurry shows that most of the prominent peaks come from the wax. The only peak missing in the wax is the α-Fe peak at 2.028 Å.

To eliminate the wax peaks and see the underlying catalyst more clearly, we tried first to concentrate the catalyst by sedimentation. These results are shown in Fig. 20 and show that the α-Fe peak is now more pronounced relative to the wax peaks. The only way we could completely eliminate the wax peaks was to heat the sample in flowing Argon at 260 °C. In this manner, most of the wax was stripped off and what was left behind was analyzed and reported as wax-stripped powder in Fig. 20. Clearly, the α-Fe peak is the only peak with a small shoulder on its left indicating some carbide is present.

In order to confirm that the single peak shown in Fig. 20 actually comes from α-Fe, we present in Fig. 21 a Reitveld refinement of the entire powder pattern for the wax-stripped sample. We can see that all of the peaks match very well the calculated pattern for α-Fe. After subtracting the α-Fe peaks, the residual pattern is shown in greater detail in Fig. 22. The peak at 2.5 Å may come from magnetite while the 2.1 Å peak could arise from the iron carbide. If one compares the relative heights of the 2.1 Å peak and that of the α-Fe peak at 2.03 Å, the unmistakable conclusion is that α-Fe is the major constituent of this sample. It must be borne in mind that the wax sample was heated in flowing Ar to get rid of the wax and obtain the wax stripped sample. If this procedure were to cause a conversion of iron carbide into α-Fe, the resulting composition profile will not represent that of the working catalyst. This is an aspect that will be studied more carefully in future work.

XRD analysis of samples in wax from run RJO-236 performed at CAER

We obtained samples from this run at various times on stream. Thus far, we have analyzed only a few of these catalysts. Three of these, taken towards the end of this run, are shown in Figs. 23 and 24. In Fig. 23, the sharp peaks and the broad hump comes from the wax . The peaks of interest occur between 35 ° and 45 ° and are shown in more detail in Fig. 24. At first glance, it is apparent that there is no magnetite present in this sample. There are several peaks in the 40 ° - 45 ° region and some of them may come from the wax, but others must represent iron carbides. α-Fe if present is seen only as a shoulder at 2.03 Å.

Future Work

Both samples analyzed by XRD show that the wax helps to preserve the catalyst to some extent against atmospheric oxidation, but only if the wax removal is performed under an inert blanket. The XRD patterns in Fig. 19 and Fig. 23 show that the wax from the Texas A&M runs in very different than the wax present in the CAER runs. It appears that the wax interferes with the XRD reflections from iron carbide, but we need to do an elemental analysis to rule out the presence of small amounts of iron carbide in the wax as it is obtained from soxhlet extraction. Our future work will investigate methods to eliminate the interference by the wax so that the true phase composition of a working F-T catalyst can be unequivocally established.

Acknowledgments
The following graduate and undergraduate students participated in this project: Linda Mansker, x-ray diffraction; Yaming Jin, F-T reactor studies and TPR; Aree Hanprasopwattana - catalyst synthesis and surface coatings; Hien Pham - attrition resistance studies, Alexander Viergutz, summer student from Cornell-spray drying. We also acknowledge helpful discussions with Dr. Mark Miller of the Earth and Planetary Sciences on Reitveld refinement methods for analysis of x-ray diffraction patterns and with Dr. Tom Rieker of the Chemical and Nuclear Engineering Department for assistance with small angle x-ray studies of titania-coated silica catalysts. The TEM and XRD measurements were performed using the analytical facilities provided by the Earth and Planetary Sciences Department.

References
1) M. J. Adams, M. A. Mullier, and J. P. K. Seville, *Powder Tech.*, **78** (1994) 5.
2) S. J. Glass and C. Newton, Symposium on Science, Technology, and Commercialization of Powder Synthesis and Shape Forming Processes, American Ceramic Society, Cincinnati, OH, 1995.

Figure 1. Temperature Programmed Reduction of the UCI unsupported catalyst in CO. Peaks corresponding to reduction of CuO --> Cu metal, hematite --> magnetite and magnetite --> α-Fe are seen. Peak identification is based on TEM analysis of samples withdrawn at various stages as well as from x-ray diffraction

Fig. 2 CO TPR of the UCI unsupported catalyst. After the first run, the sample was oxidized and a second TPR was run. TEM analysis was performed as indicated by arrows. These TEM images are presented in the following figures.

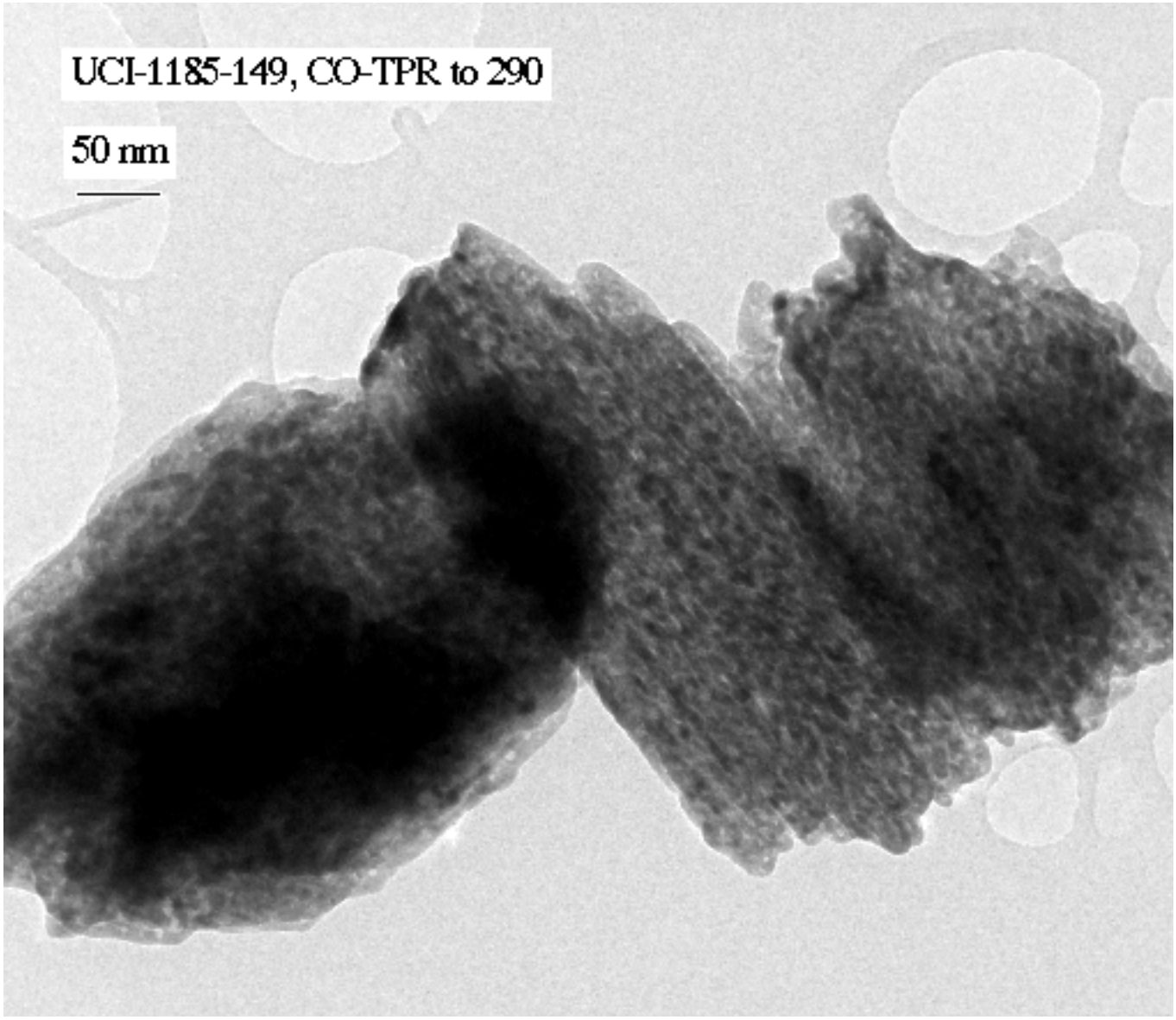

Figure 3a Low magnification view of UCI unsupported catalyst after CO TPR up to 290 °C. The "Swiss-cheese" morphology of the hematite catalyst is preserved, however the catalyst has completely transformed into magnetite

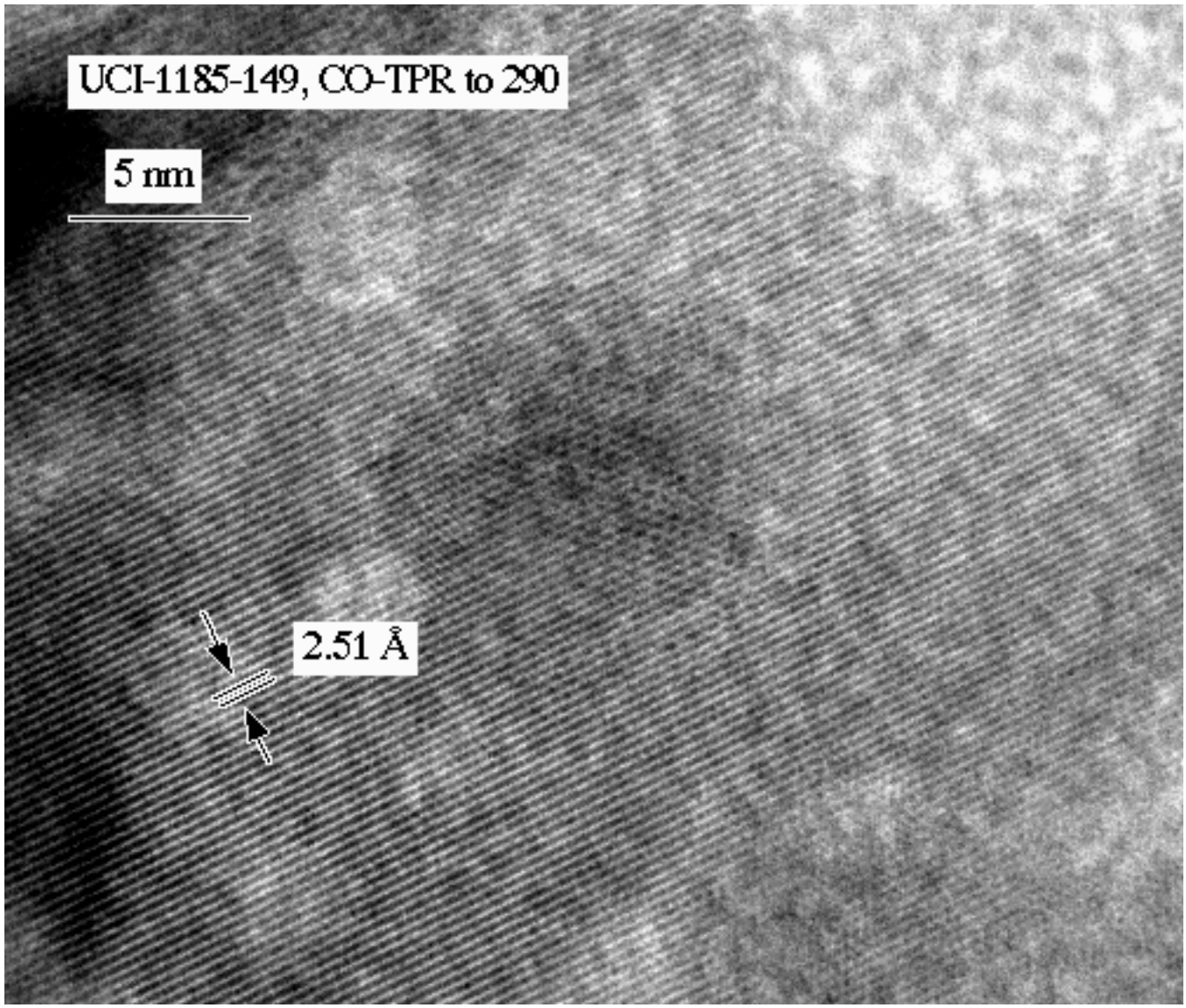

Fig. 3b Higher magnification view of the catalyst shown in Fig. 3a. Lattice fringes corresponding to magnetite can be clearly seen. The individual particles are single crystals.

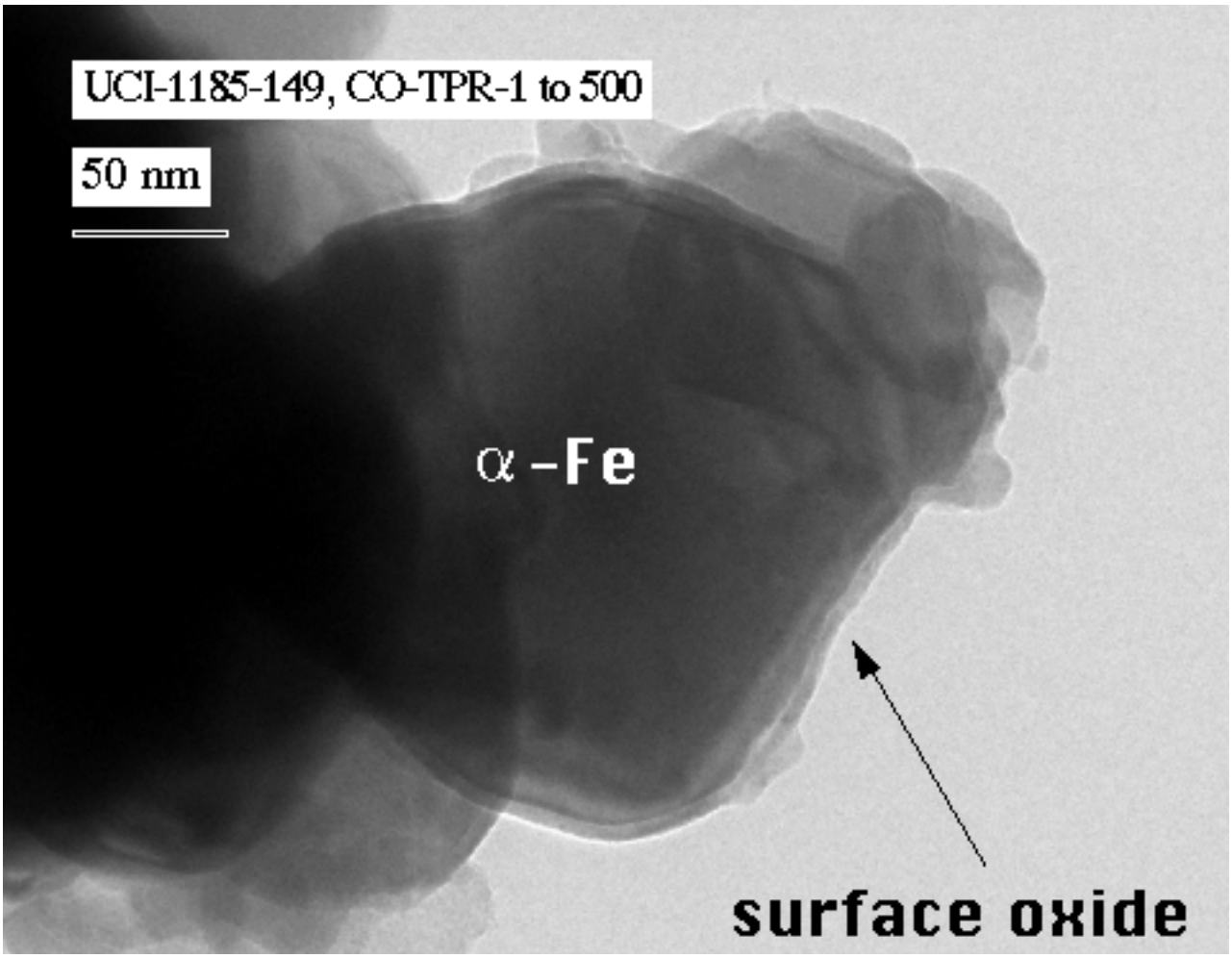

Fig. 4a Low magnification view of UCI catalyst after CO TPR to 500 °C. Large metallic particles of α-Fe are seen. The surface oxide is caused by exposure to air during transfer to the electron microscope. What is surprising is the absence of any amorphous carbon or graphite considering that the sample was reduced in CO at 500 °C.

Fig. 4b (on the next page) shows an electron diffraction pattern from this sample. The large Fe particles give rise to the diffraction spots while the surface oxide (magnetite) gives a diffuse ring pattern.

Fig. 4c (on the next page) shows a higher magnification view of the α-Fe crystals showing lattice fringes.

b

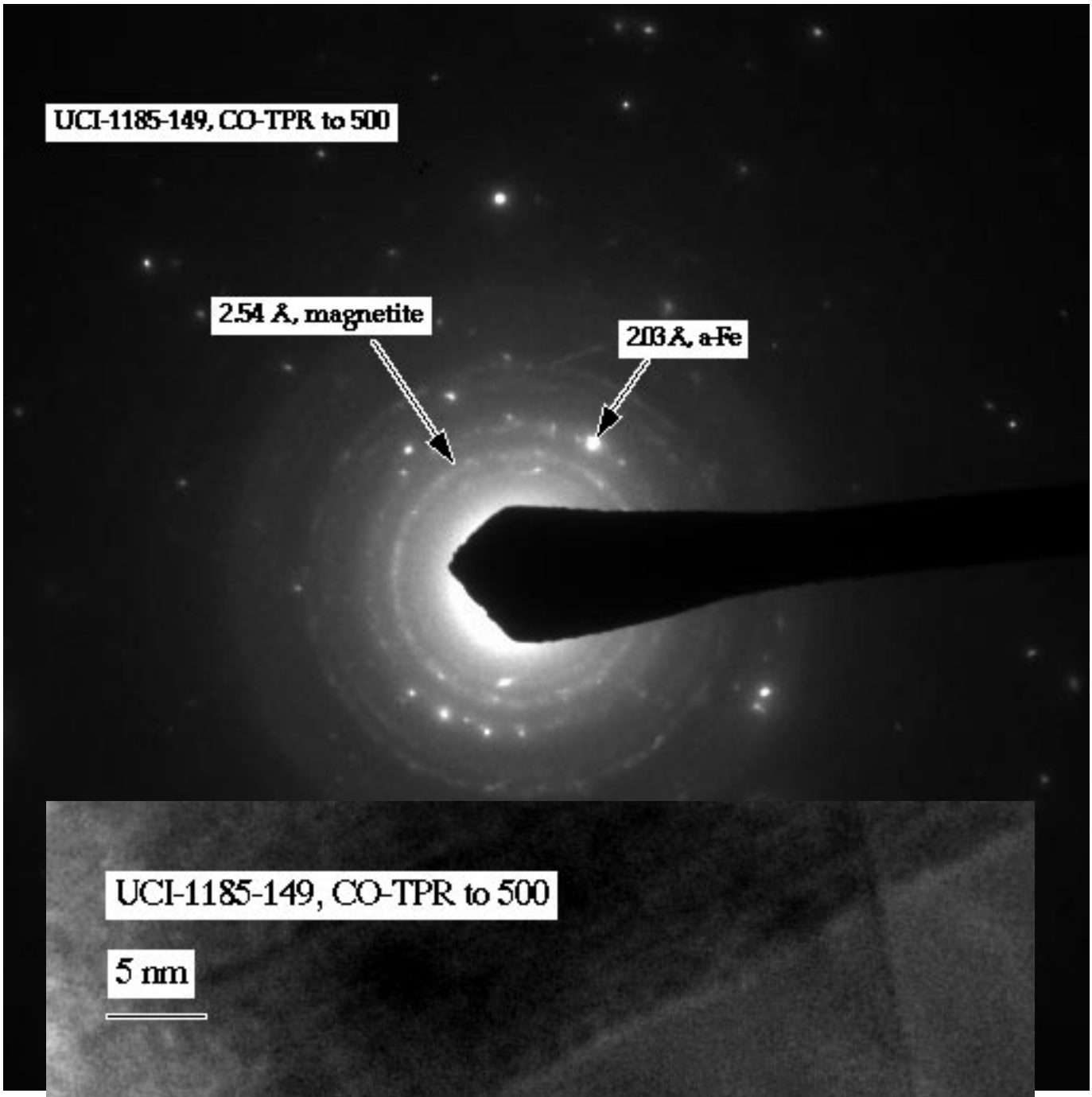
UCI-1185-149, CO-TPR to 500
2.54 Å, magnetite
2.03 Å, a-Fe

c

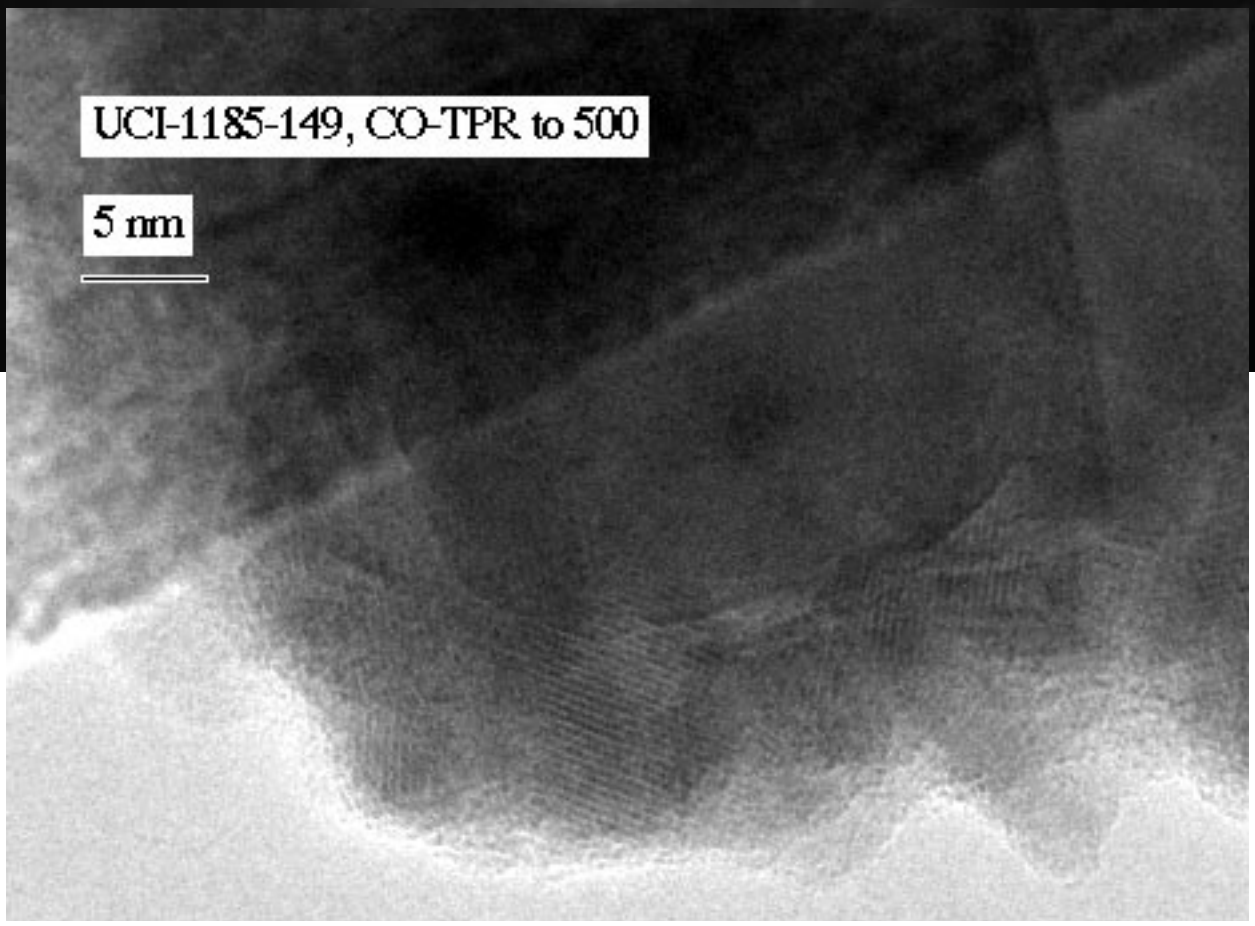
UCI-1185-149, CO-TPR to 500
5 nm

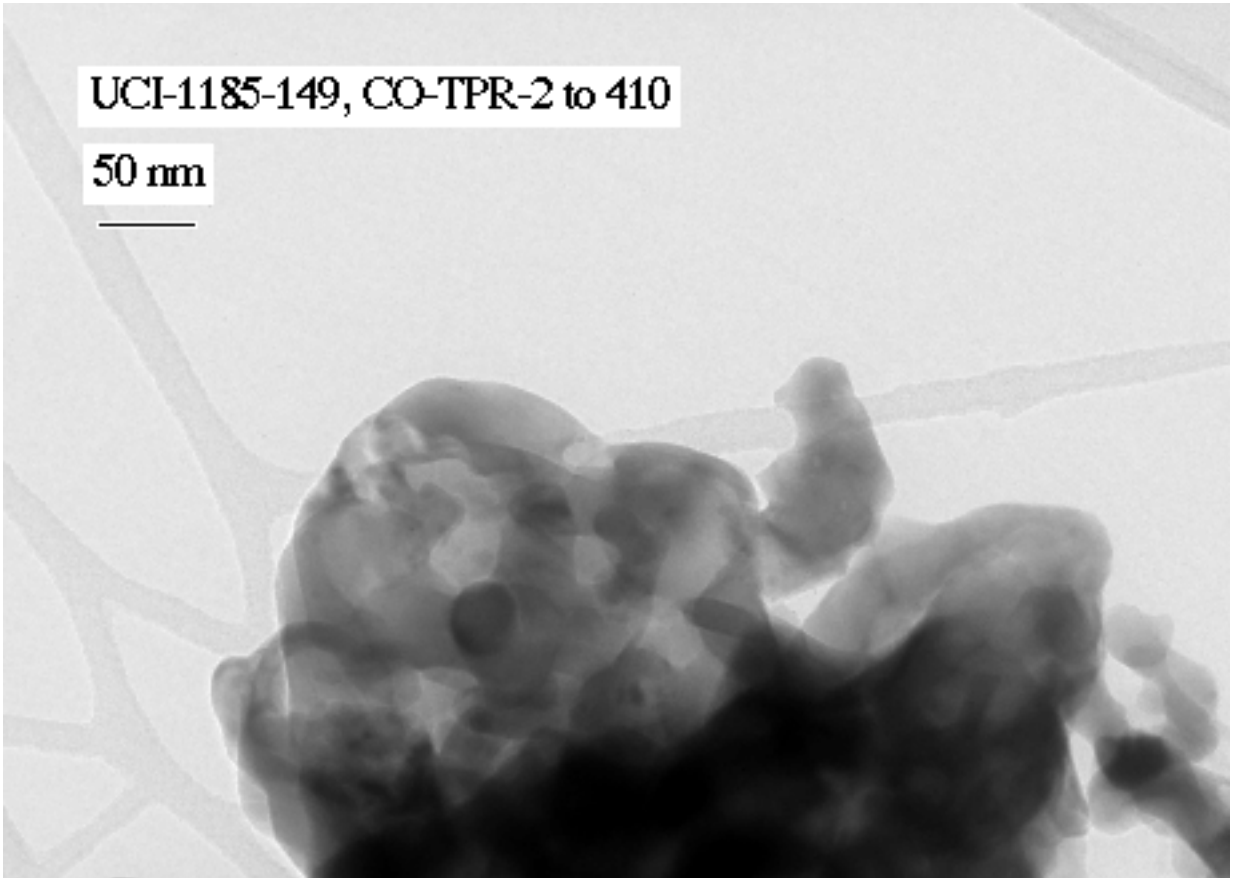

a

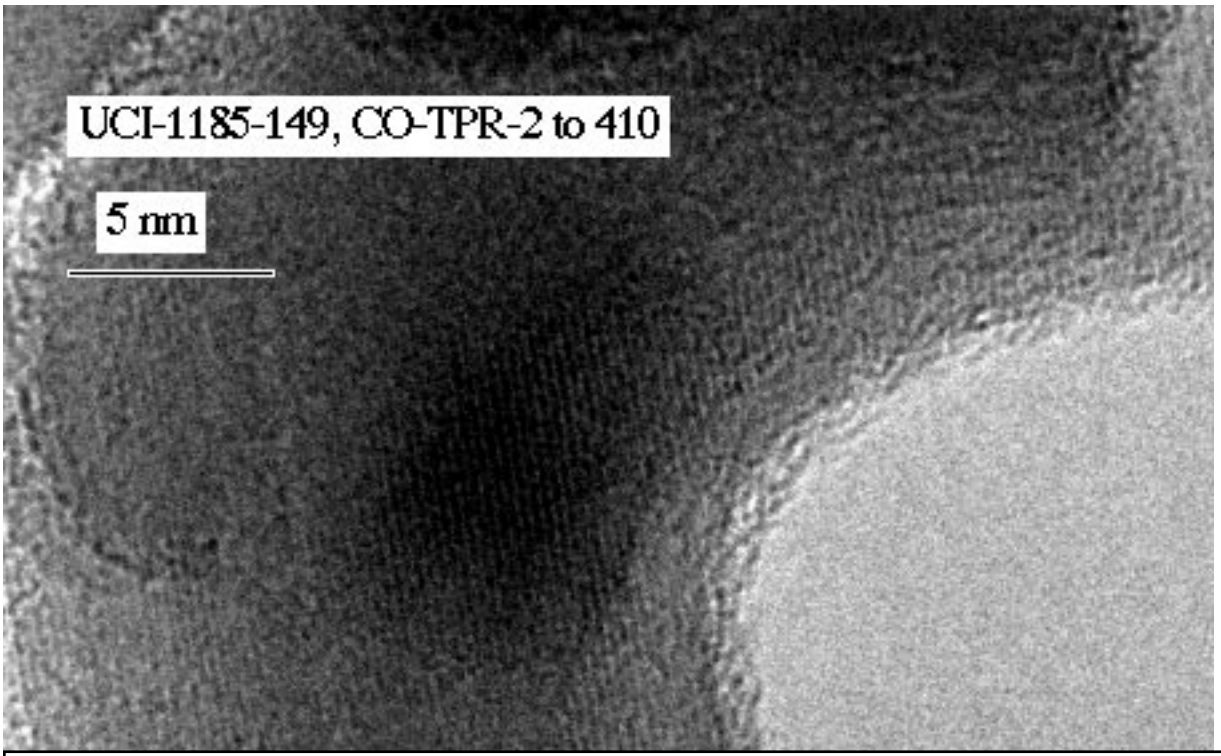

b

Figure 5 TEM of UCI catalyst during the 2nd TPR (i.e. after reduction in CO, oxidation at 500 °C). Low mag view (a) and Higher magnification view (b). Note the magnetite is much more dense than the one in Fig. 3 explaining the higher temperature required for reduction.

TEM pictures of unsupported UCI catalyst after CO-TPR

---transformation to α-Fe with a surface passivation layer,

---no carbide;sintering of metal particles

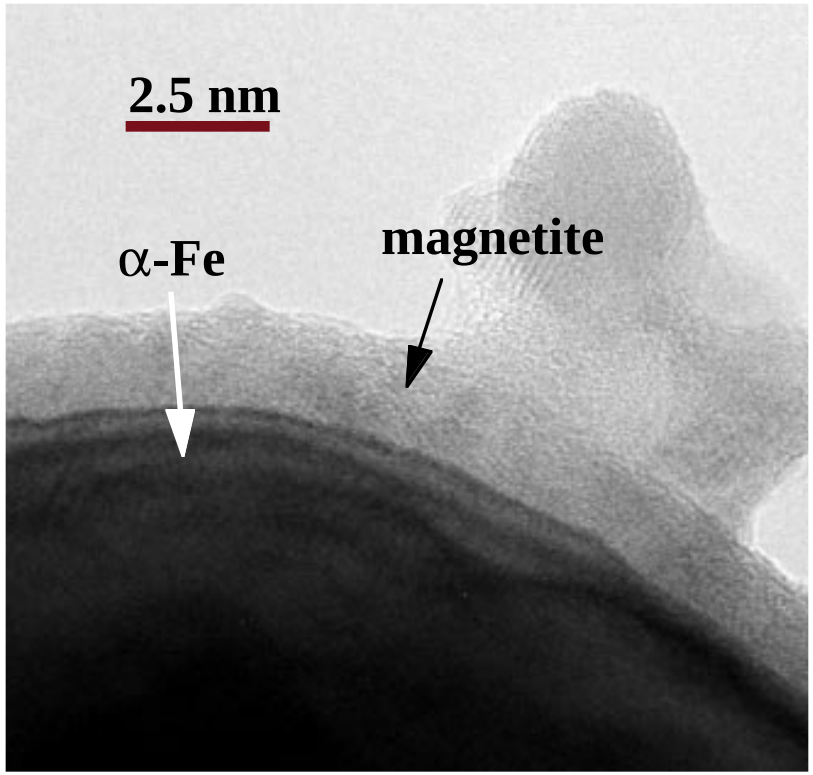

high mag. picture

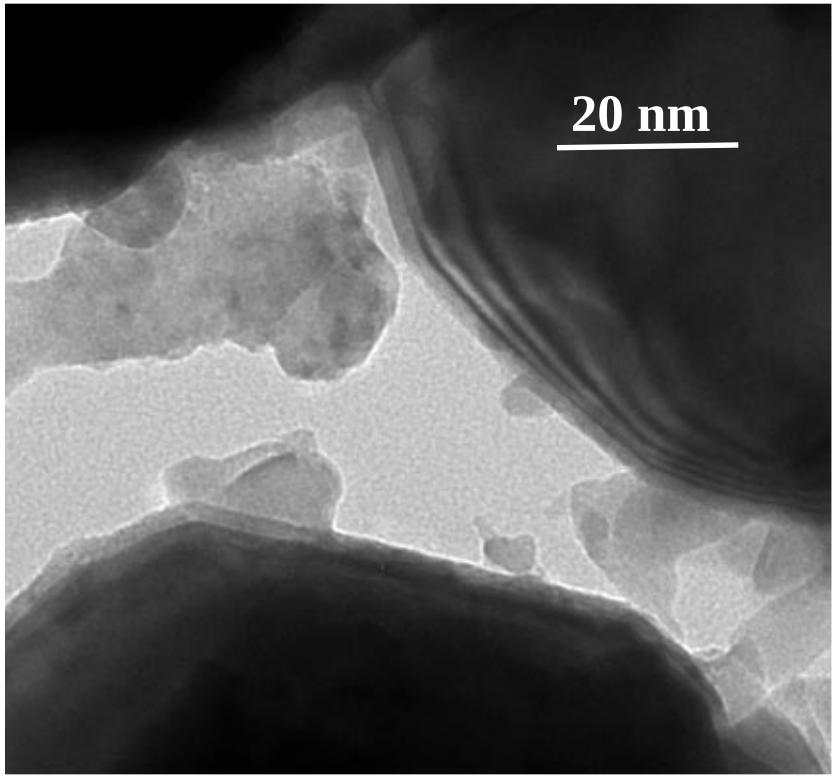

low mag. picture

Fig. 6 TEM after 2nd CO TPR of UCI unsupported catalyst. There is no evidence of any any carbonaceous species being present on the surface.

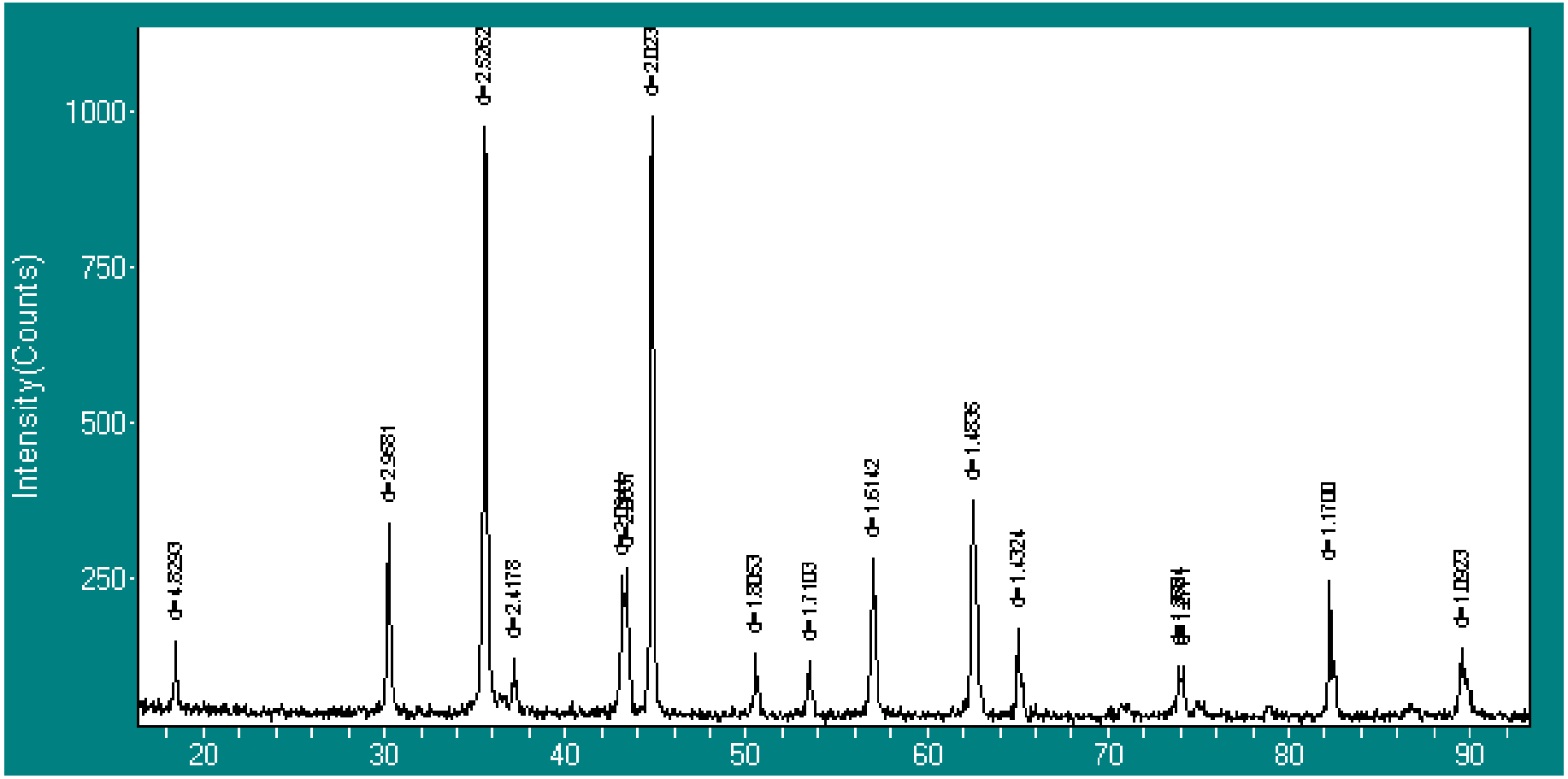

Fig. 7 X-ray diffraction pattern of the UCI catalyst after 2nd CO TPR. For this experiment, we used 0.120 g of sample instead of 0.020 g as in a typical TPR run. Hence the extent of reduction of the magnetite maybe somewhat less than in a conventional TPR experiment. Nonetheless, the xrd pattern shows clearly that under conditions of CO TPR where temperature is ramped at 10 °C/min, an unsupported Fe, Cu catalyst transforms into α-Fe instead of into iron carbide. This is in contrast to the behavior of a supported Fe, Cu catalyst shown in Figures 8-11 where it is seen that the catalyst directly transforms into iron carbide without an identifiable α-Fe transitional phase. We believe that the smaller particle size of the magnetite in the supported catalyst facilitates trasnformation into iron carbide.

Fig. 8 CO TPR of a supported Fe(Cu) catalyst. The catalyst support consists of microspheres of silica. Three peaks are seen, first hematite --> magnetite, second magnetite --> iron carbide and the third corresponding to the Boudouard reaction CO --> C(surface) + CO_2. Peak identification is based on TEM images shown in Fig. 9 and 10 and on the x-ray diffraction pattern in Fig. 11.

TEM picture of Fe(Cu)-supported after CO-TPR to 380°C

Diffuse spot diffraction pattern from iron carbide polycrstals

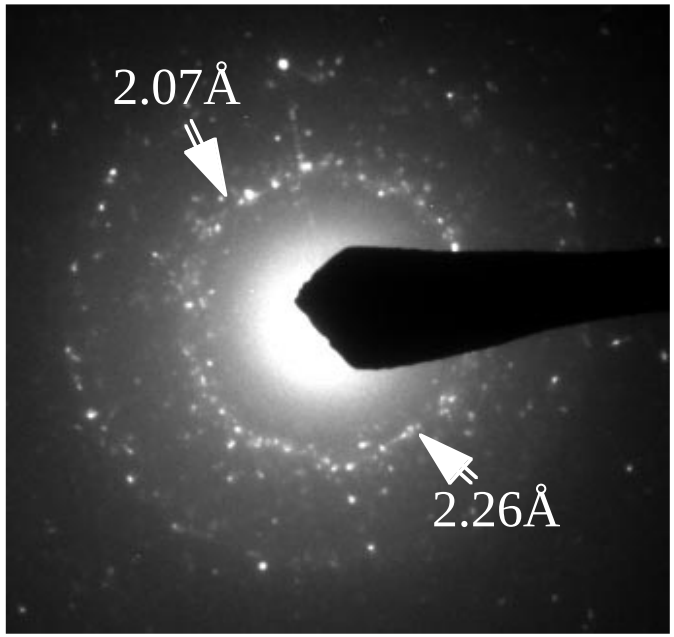

electron diffraction pattern

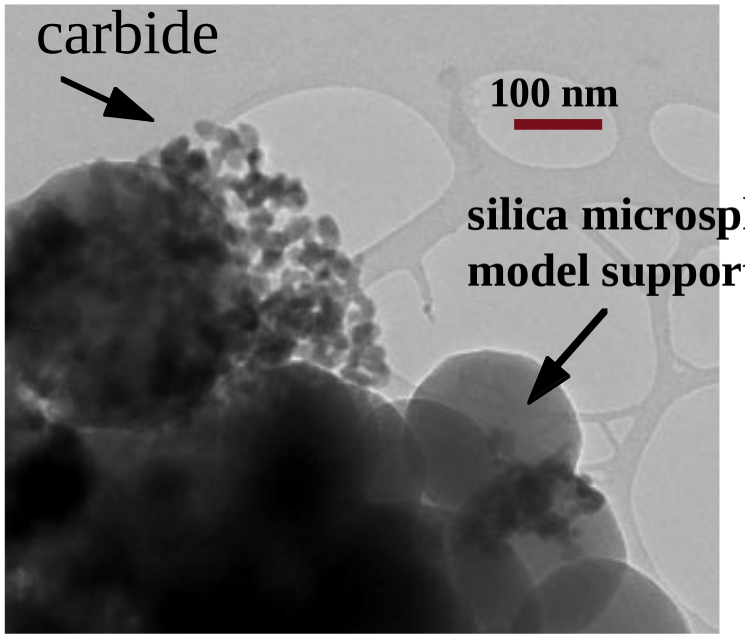

low mag. picture

Fig. 9a) Electron Diffraction pattern and b)Low magnification image of the Cu promoted, Fe catalyst. The model silica support makes it easier to study the morphology of the Fe catalyst. After CO TPR to 380 °C small crystals of iron carbide are seen. The carbide is identified from its electron diffraction pattern and the XRD pattern (Fig. 10) of this sample.

HRTEM of Fe(Cu)-supported catalyst CO-TPR to 380°C

Small iron carbide particles surrounded by a layer of amorphous carbon

No oxide layer because of carbon layer protection

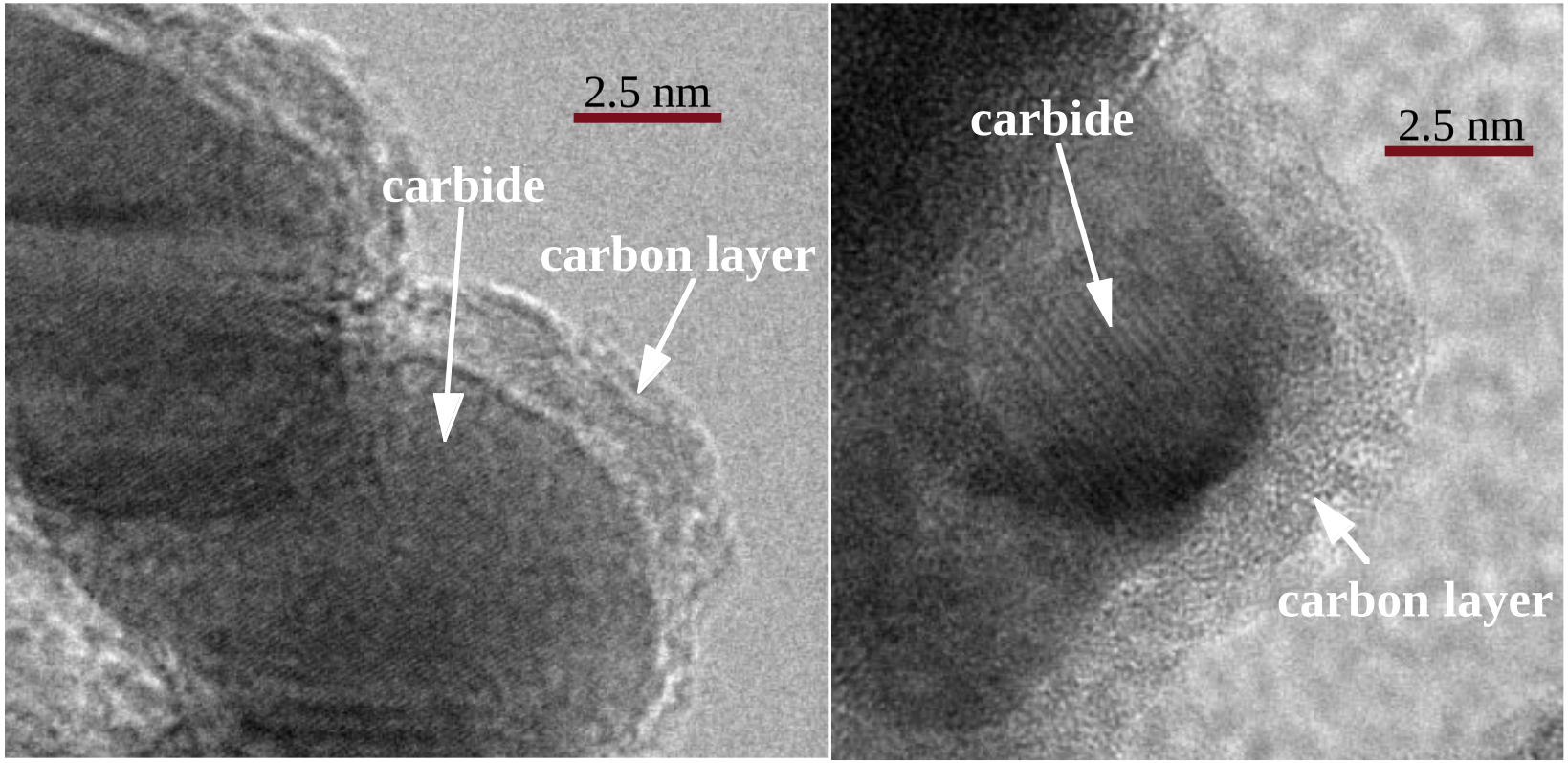

Fig. 9(contnued). c) and d) These are higher magnification views of the sample seen on the previous page. The carbide particles show amorphous carbon being present on the particle surface (in contrast to the α–Fe particles in Fig. 4 and 6) that show only a surface oxide being present. In this sample, the amorphous carbon prevents oxidation of the catalyst.

TEM picture of Fe(Cu)-supported after CO-TPR to 500 °C

3.32Å d-spacing coresponding to graphite, diffuse spots around 2Å from carbide

The higher temperature causes significant deposition of carbon, as graphite.

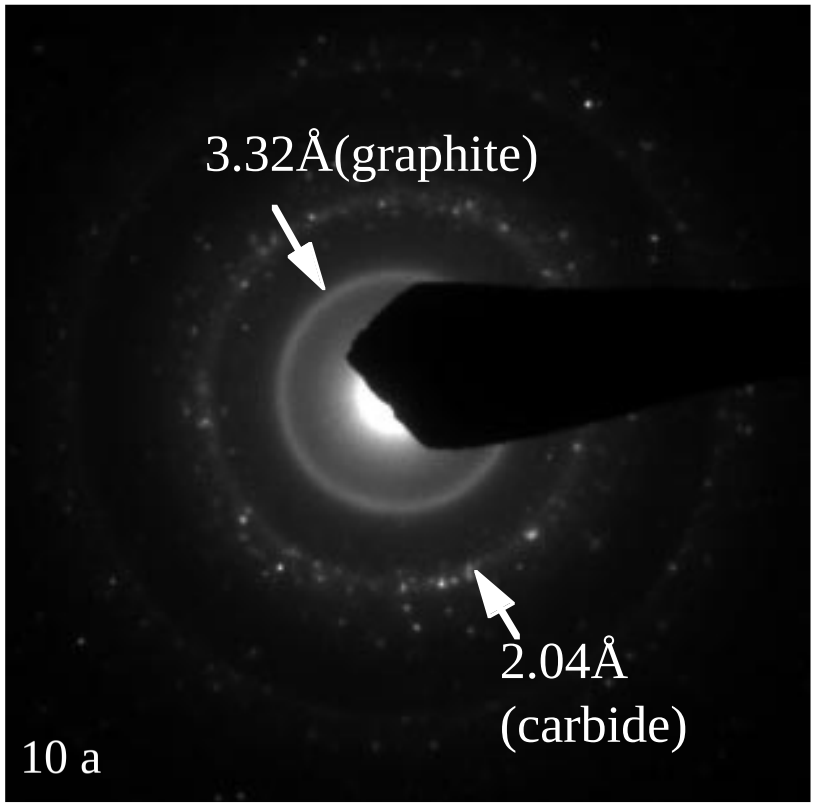

electron diffraction pattern

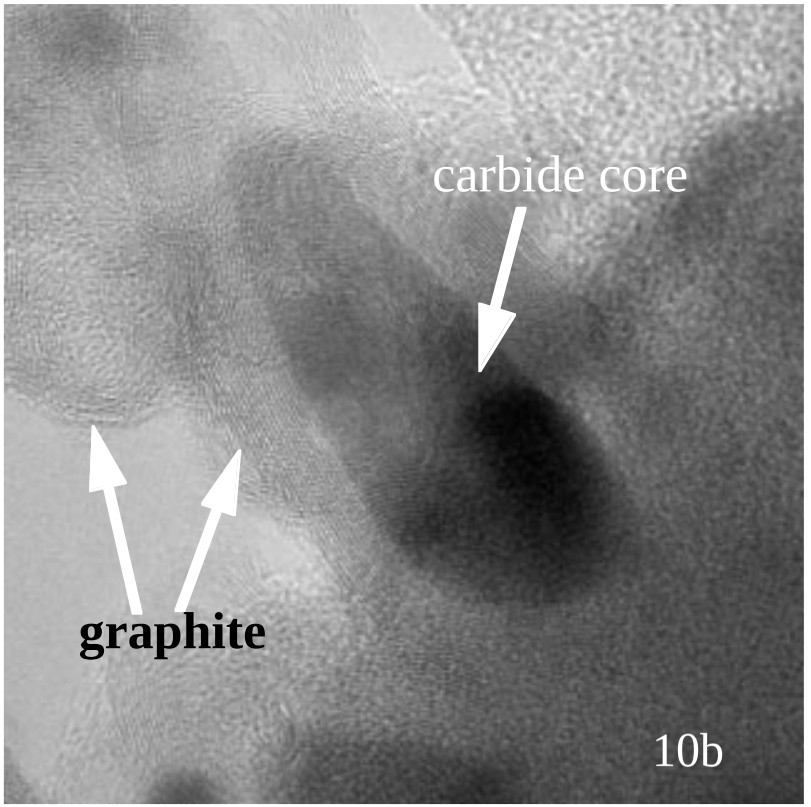

high mag. picture

TEM pictures of Fe(Cu)-supported catalyst after CO-TPR

A lot of carbon deposition and the carbon layer provides protection of underneath carbide against oxidation, no magnetite is observed

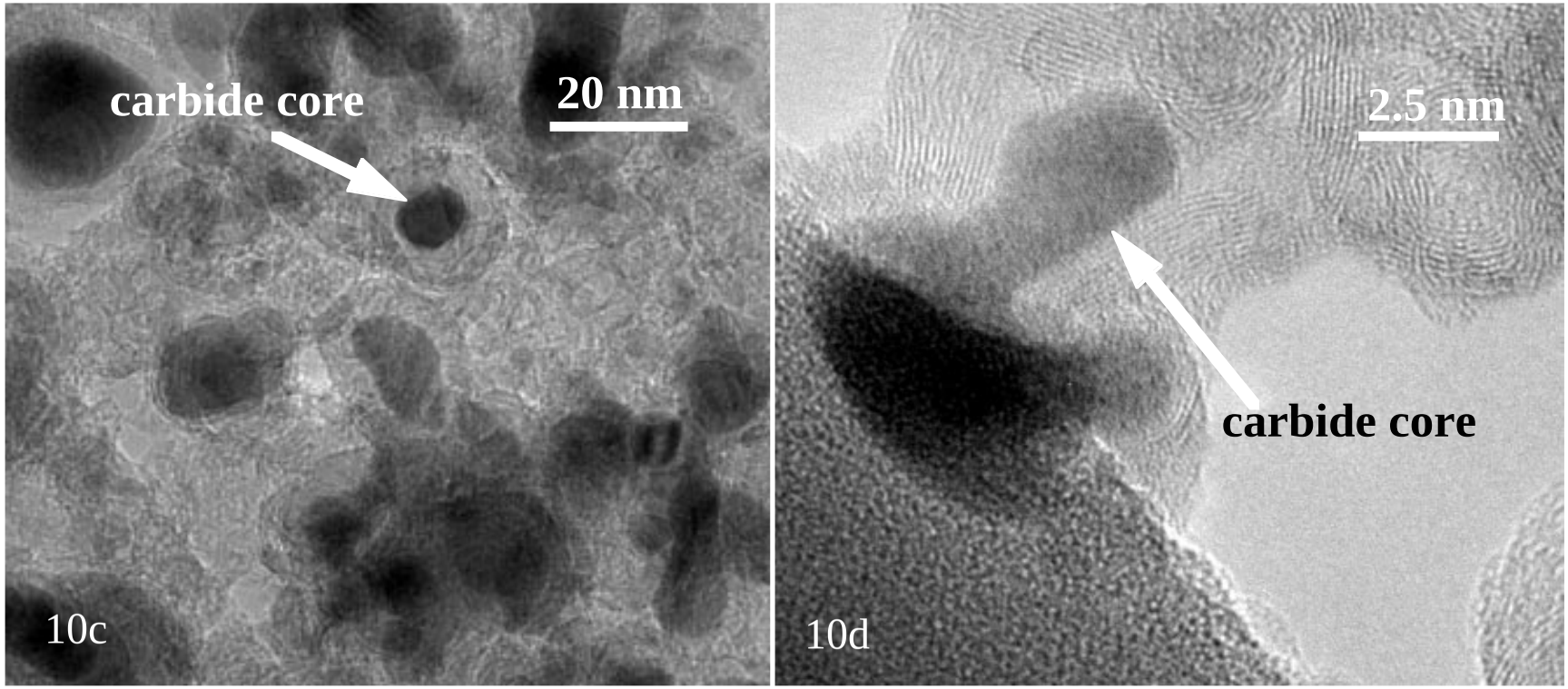

low mag. picture

high mag. picture

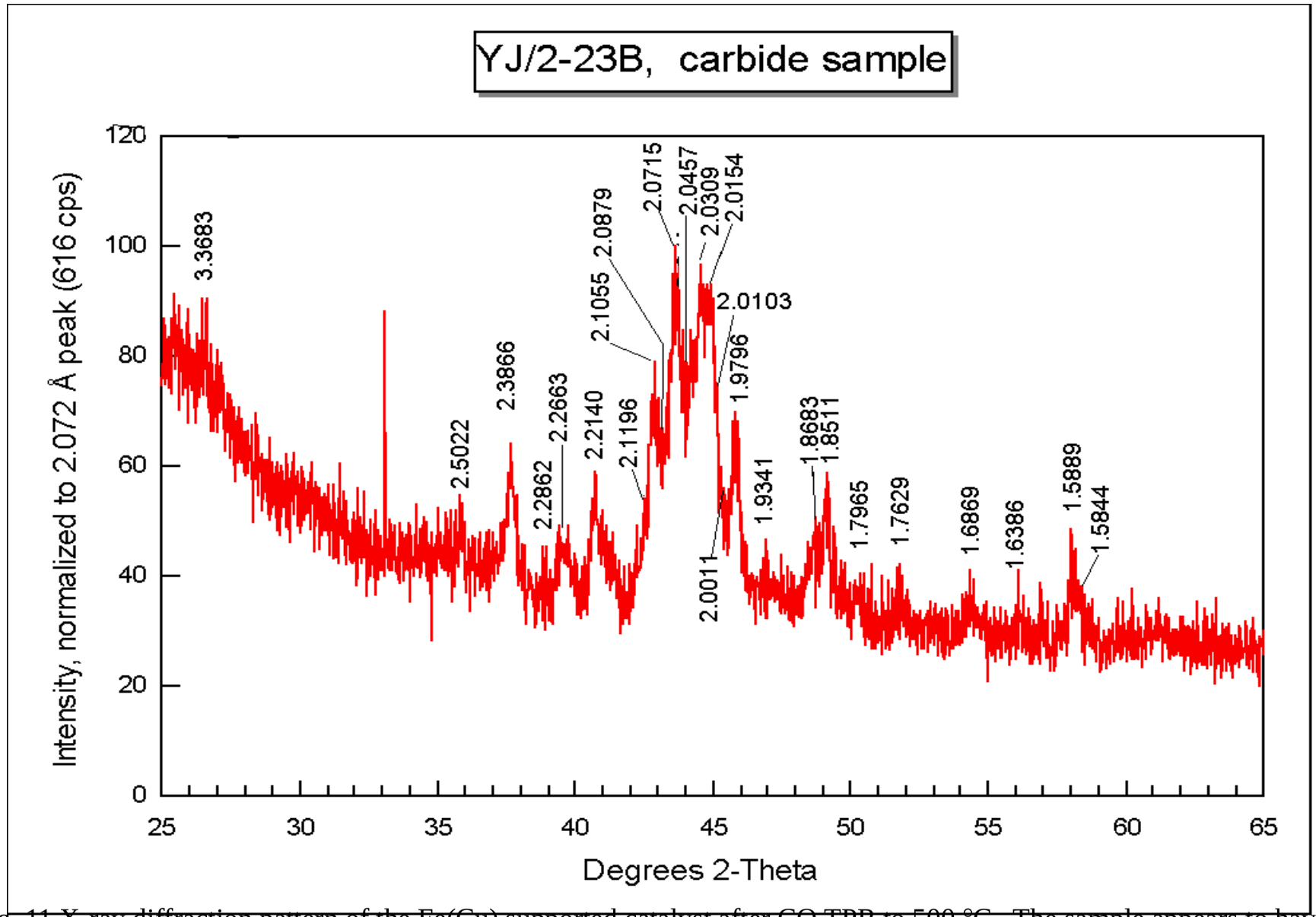

Fig. 11 X-ray diffraction pattern of the Fe(Cu) supported catalyst after CO TPR to 500 °C. The sample appears to have transformed completely to carbide. No magnetite is seen by XRD, which is consistent with the TEM images shown in Figures 9 and 10, where the carbonaceous layers on the surface helps protect the carbide from oxidation.

12 a

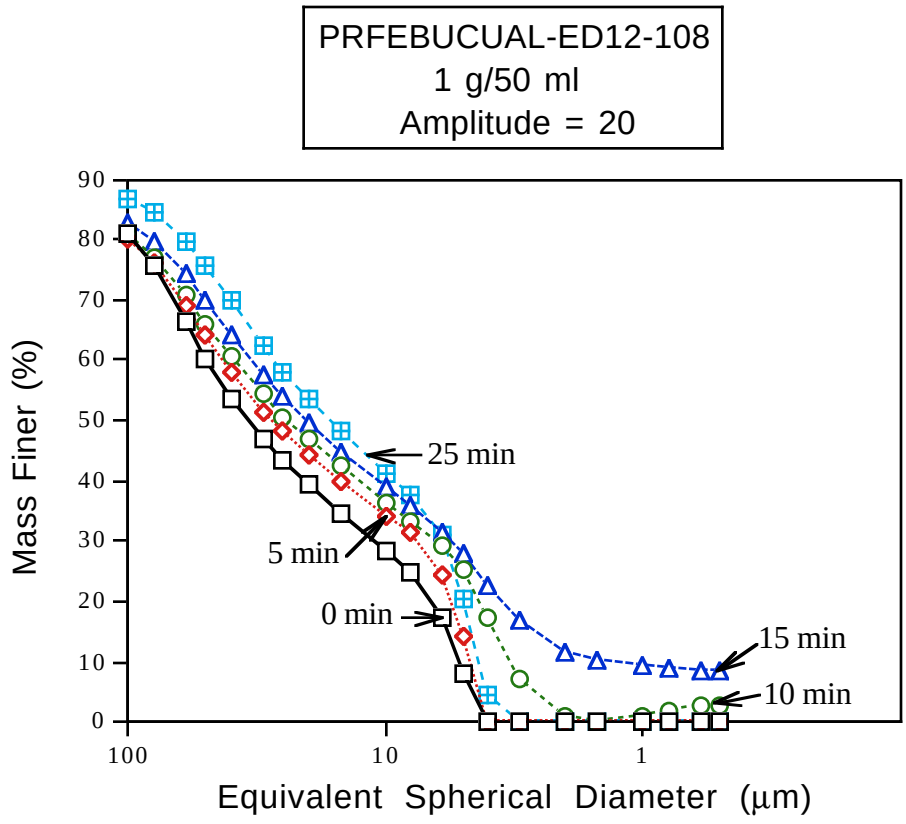

Fig. 12 Ultrasonic Fragmentation results for catalyst PRFECUBUAL-ED12-108 (12 a), PRFECUAL4K-ED12-112 (12 b, next page) and PRFECUPRAL/4K-ED11-117 (12c, next page) prepared by Robert Gormley, FETC. Samples 112 and 117 have had K added and had been calcined at 350 °C and appear comparable in strength to the uncalcined sample 108. These results suggest that calcination at this temperature does not result in a significant increase in agglomerate strength compared with the uncalcined sample.

12 b

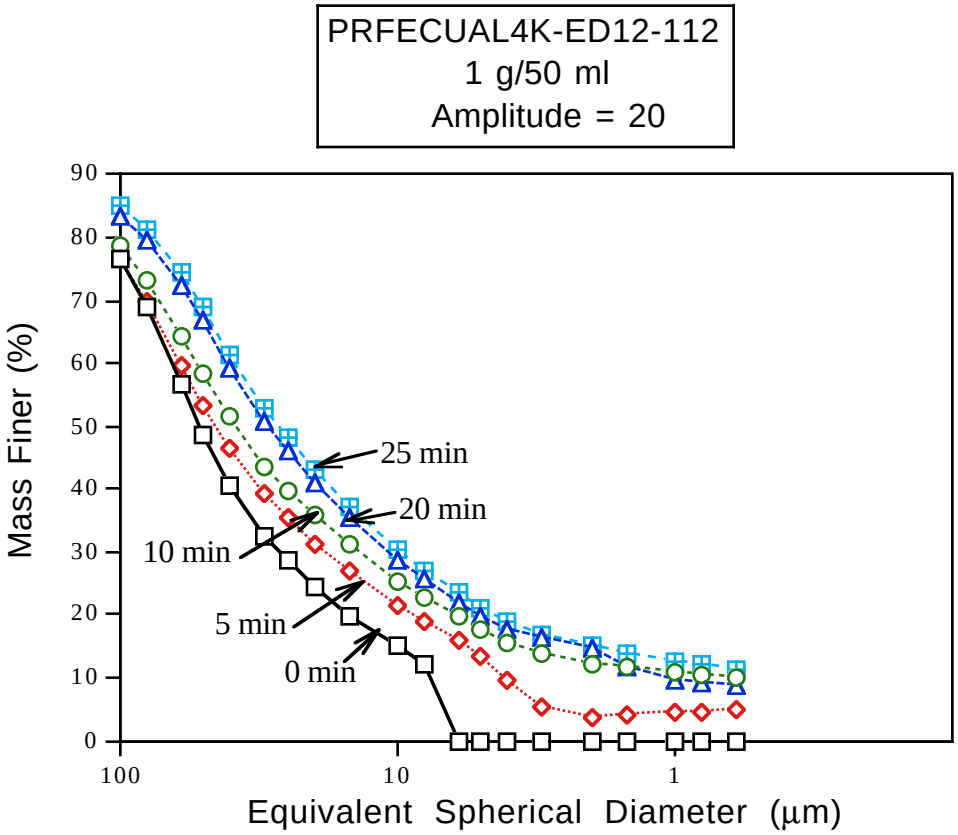
PRFECUAL4K-ED12-112
1 g/50 ml
Amplitude = 20
Mass Finer (%)
90
80
70
60
50
40
30
20
10
0
25 min
20 min
10 min
5 min
0 min
100
10
1
Equivalent Spherical Diameter (µm)

12 c

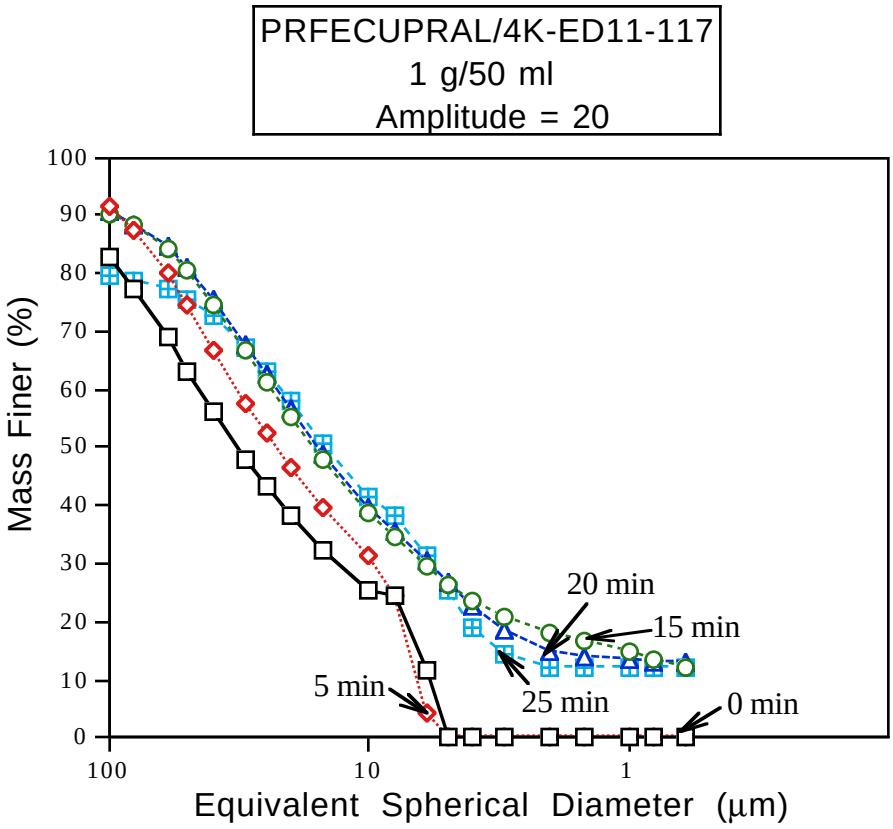
PRFECUPRAL/4K-ED11-117
1 g/50 ml
Amplitude = 20
Mass Finer (%)
100
90
80
70
60
50
40
30
20
10
0
20 min
15 min
5 min
25 min
0 min
100
10
1
Equivalent Spherical Diameter (µm)

13 a

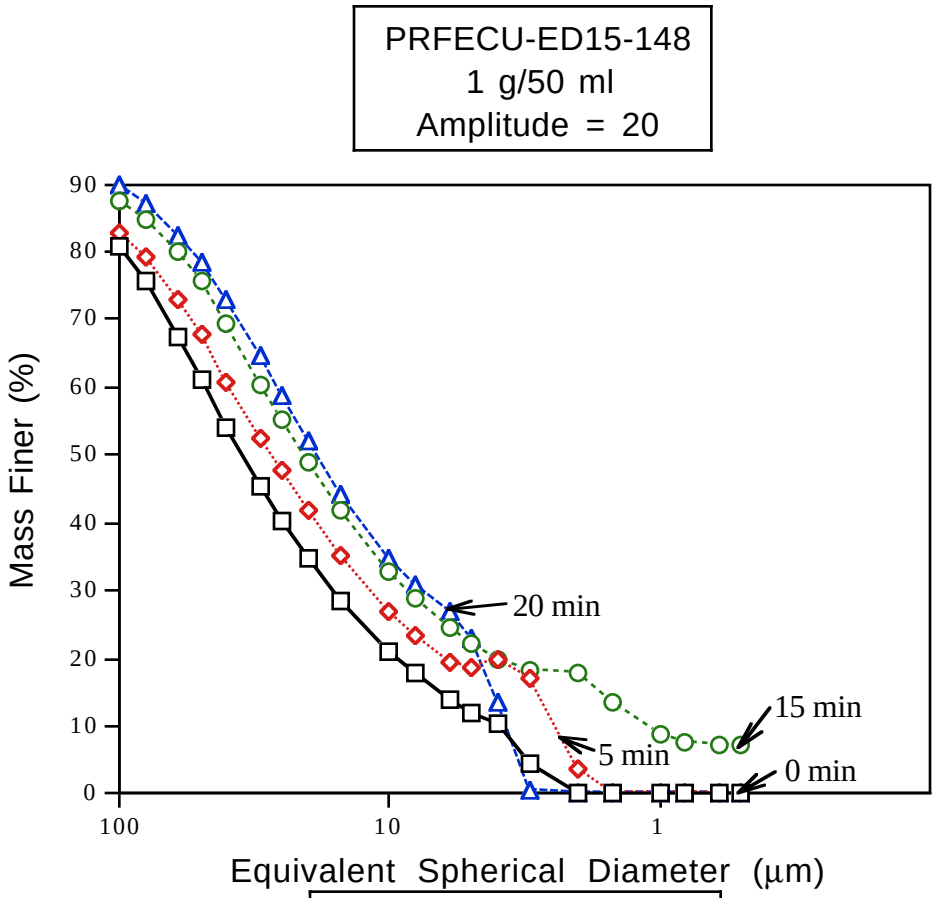

13 b

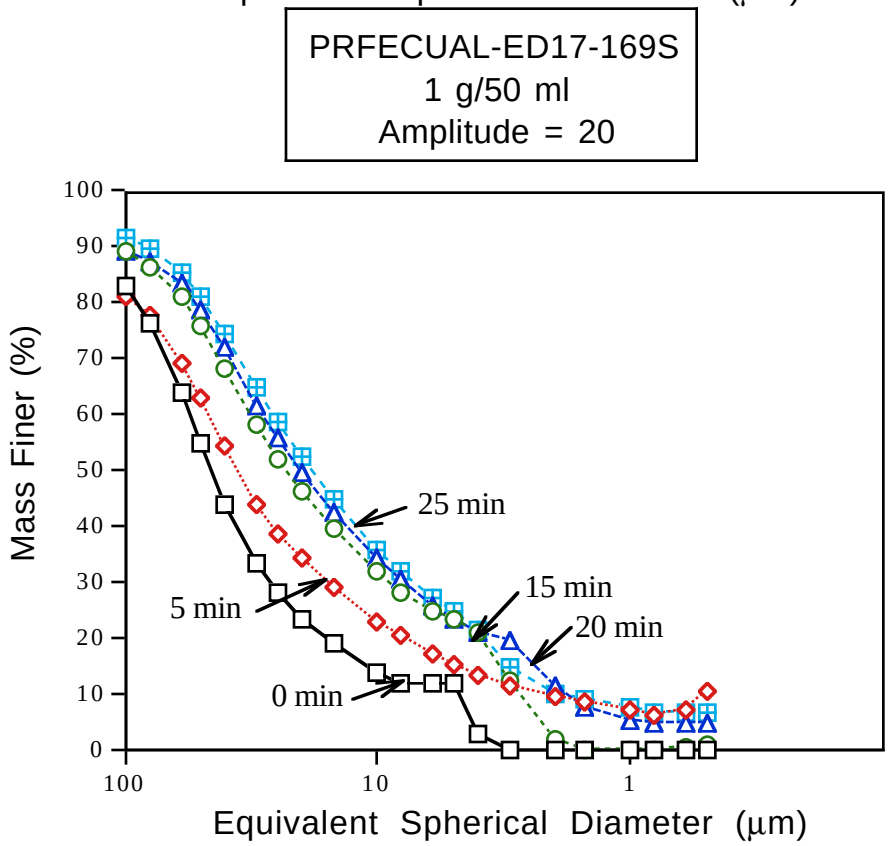

Fig. 13 Ultrasonic fragmentation results for a precipitated Fe catalysts prepared by Robert Gormley at FETC. Fig. 13 a shows a co-precipitated Fe-Cu oxide catalyst, while 13 b represents a co-precipitated Fe-Cu-Al oxide catalyst with the -400 mesh fines removed. Both had no K added and were uncalcined. The alumina does not appear to impart any additional strength to the powder.

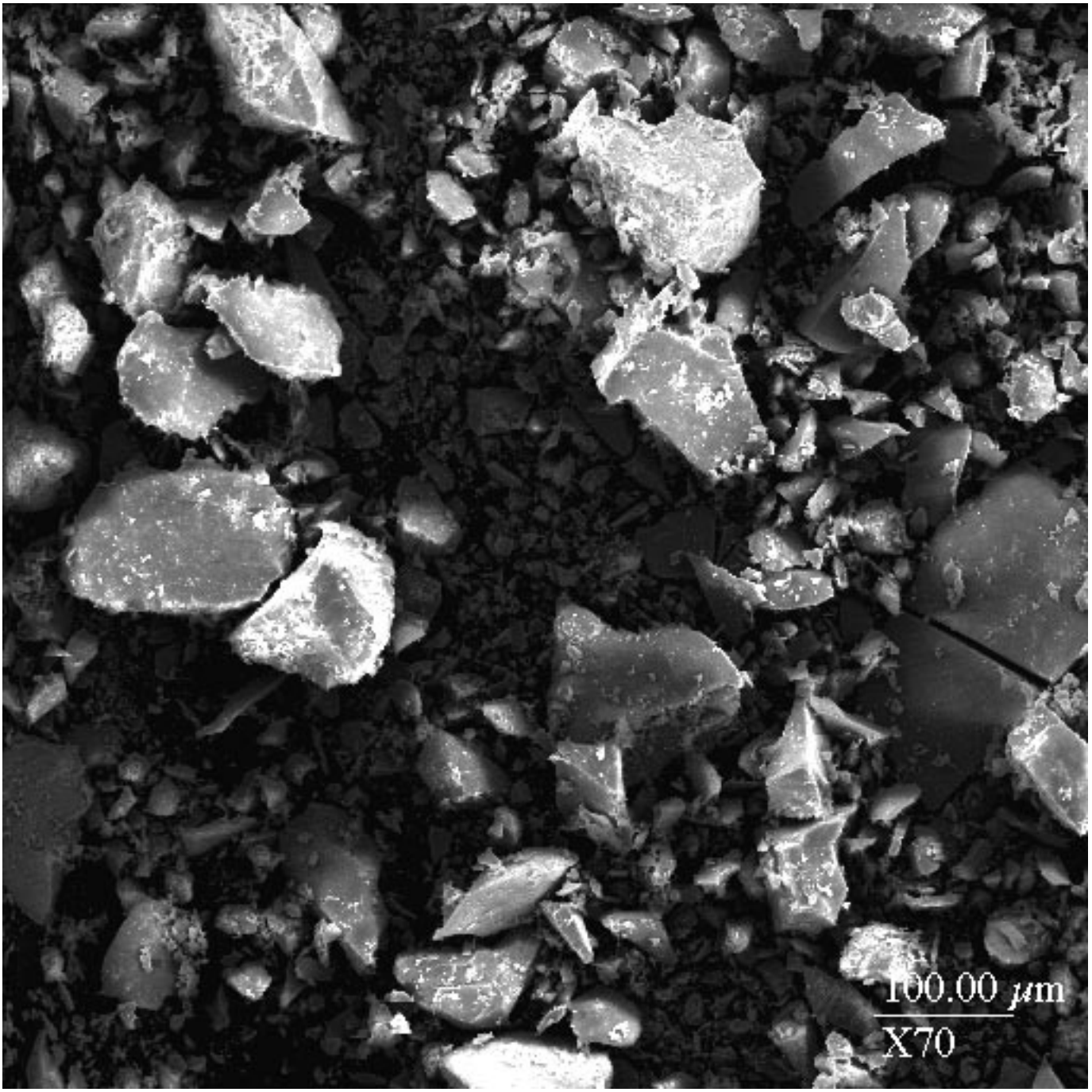

Fig. 14 Scanning Electron Micrograph of sample PRFECU-ED15-148 whose ultrasonic fragmentation results were presented on the previous page. The catalyst was prepared by Robert Gormley at FETC and is a precipitated Fe, Cu catalyst dried in vacuum at 110 °C. The catalyst is composed of irregularly shaped agglomerates. As seen from Fig. 13, these agglomerates are quite strong but they have a rather broad size distribution with a significant amount of fine particles.

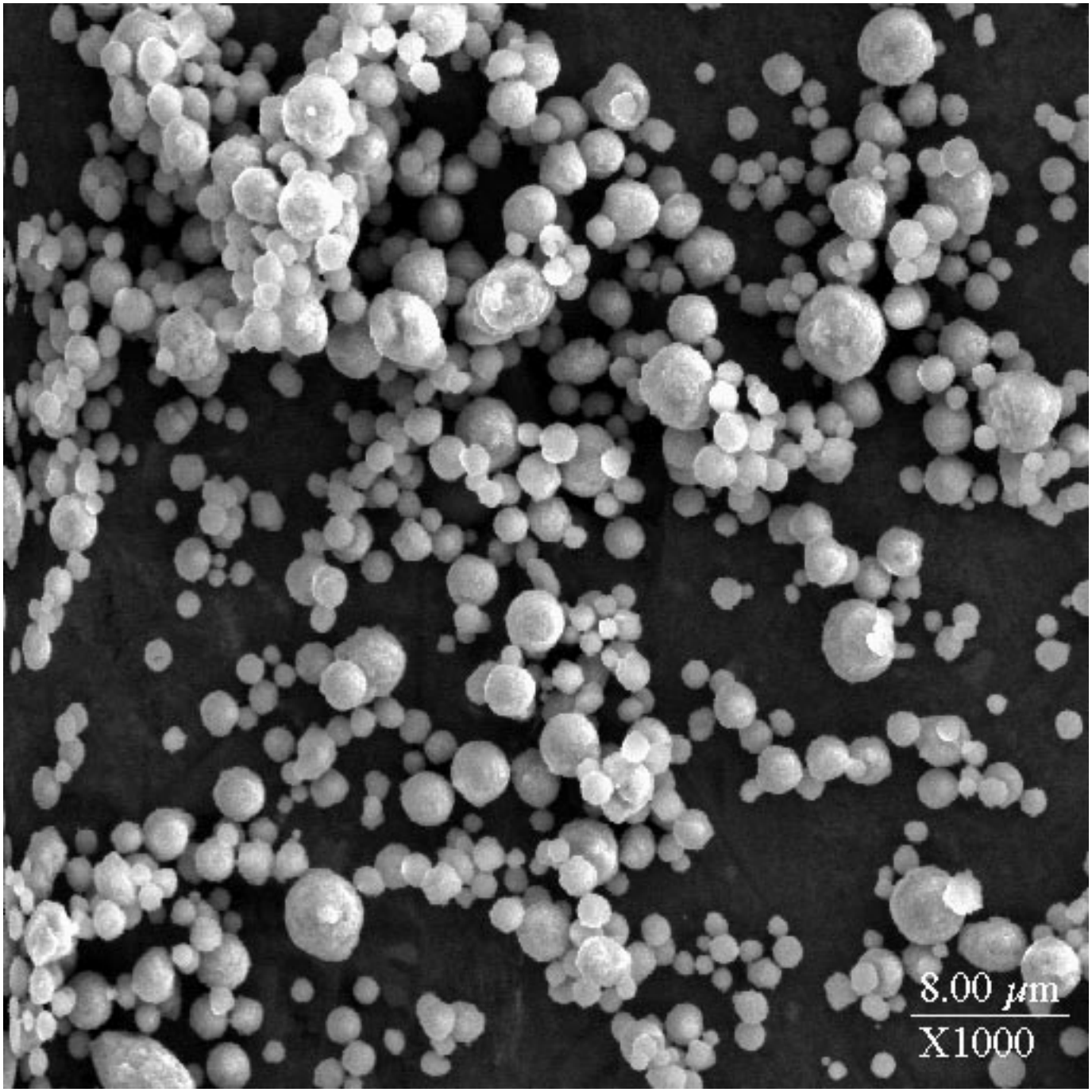

Fig. 15 Scanning Electron Micrograph of a precipitated Fe, Cu, K catalyst spray dried at UNM with a silica binder. Spherical particles typical of a spray dried powder can be seen. Ultrasonic fragmentation results on this sample are presented on the next page.

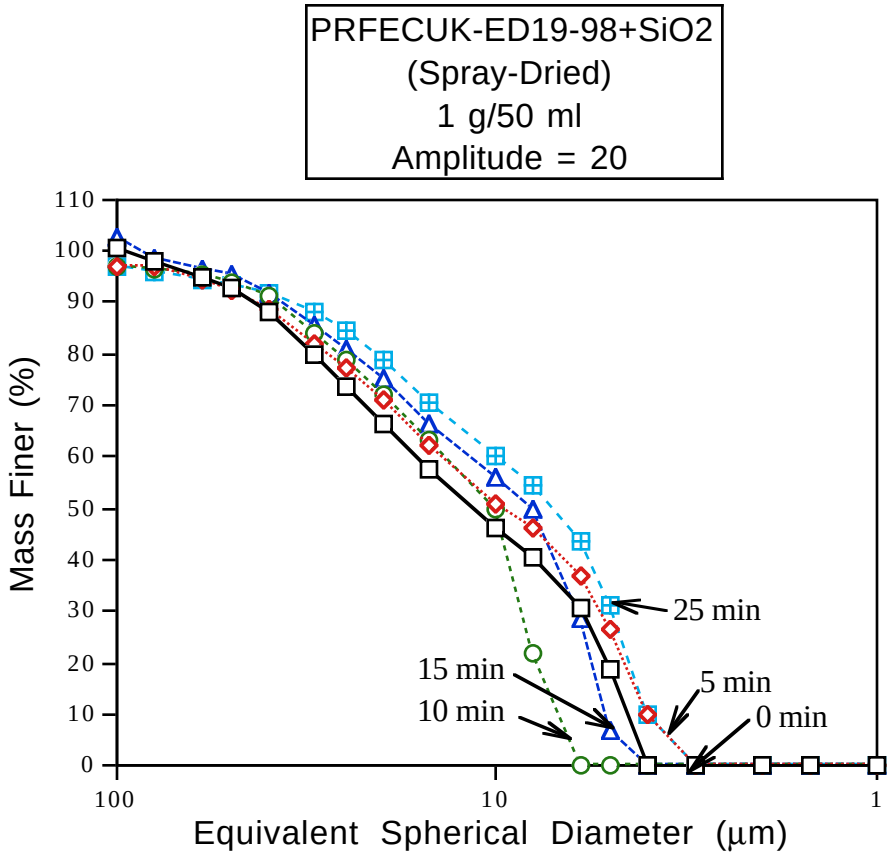

Fig. 16 Ultrasonic fragmentation results for the spray dried powder shown in Fig. 15. For comparison, fragmentation results obtained with the base case Fe catalyst (used for Laporte I) and a Vista alumina catalyst support are shown on the next page (reproduced from our Feb 1997 progress report). The spray dried Fe catalyst (shown above) appears to be comparable in strength to the alumina support (17 b).

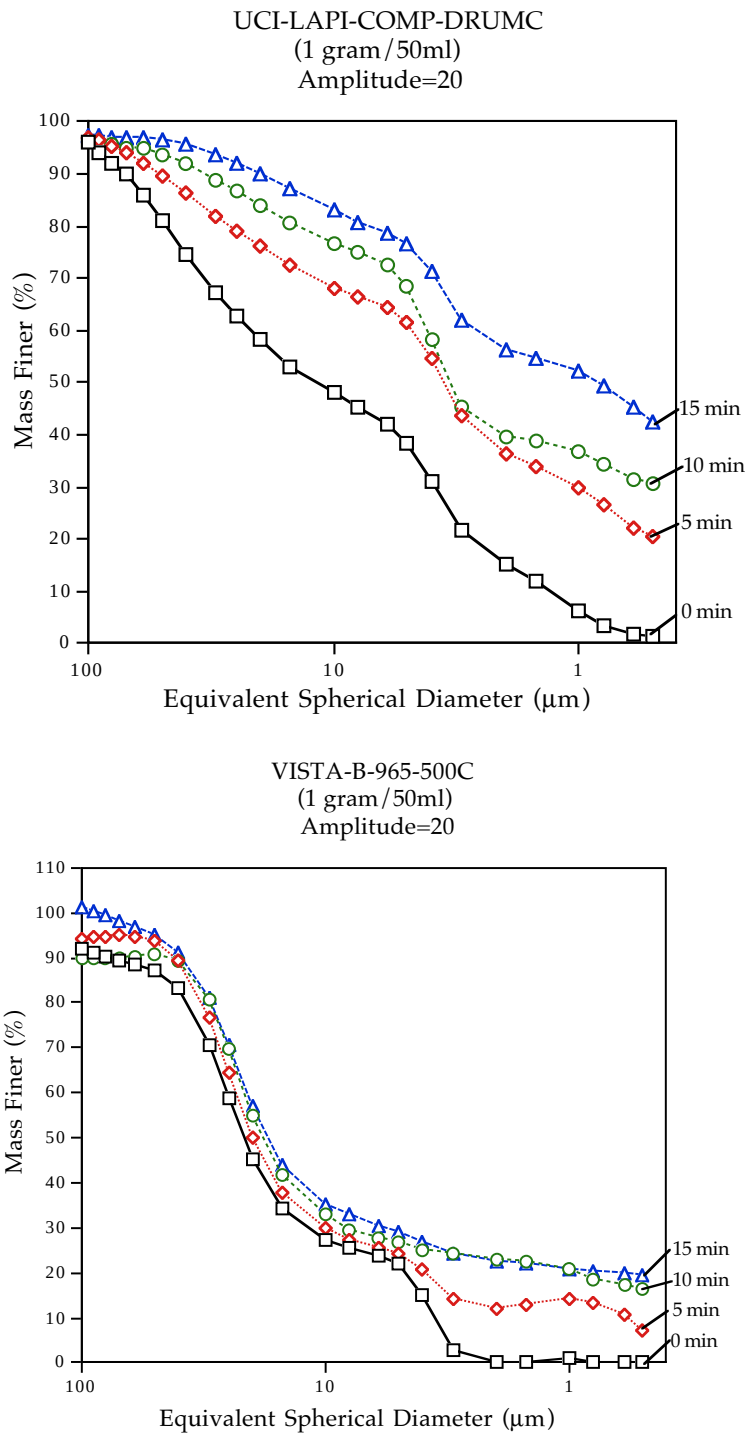

Fig. 17 Comparison of the ultrasonic fragmentation of the Fe base catalyst and a commercial alumina support. The Fe catalyst appears to break down by particle rupture as well as erosion, while erosion is the only mechanism occurring with the alumina support. Compaction tests for these two catalysts are shown in Fig. 18

18 a

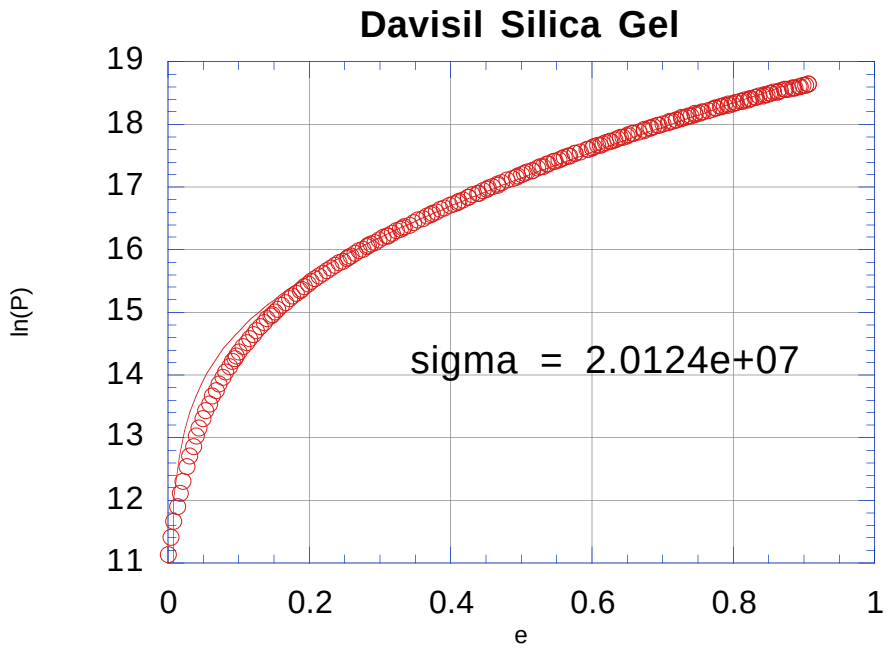

Figure 18 Compaction tests of three catalyst powders
a) Davisil silica gel (strength = 20.12 MPa)
b) Fe catalyst used for Laporte I (strength = 6.3 MPa)
c) Vista alumina support (strength = 7.4 MPa)

Davisil silica appears to have the strongest particles while the Vista alumina and the Fe catalyst are comparable. Note that the Davisil silica is not spray dried and while the strengths of the alumina and Fe catalysts are similar, their fragmentation behavior shown in Fig. 17 is very different. The Fe catalyst shows significant breakdown at energies where the alumina only exhibits mild erosion.

18 b

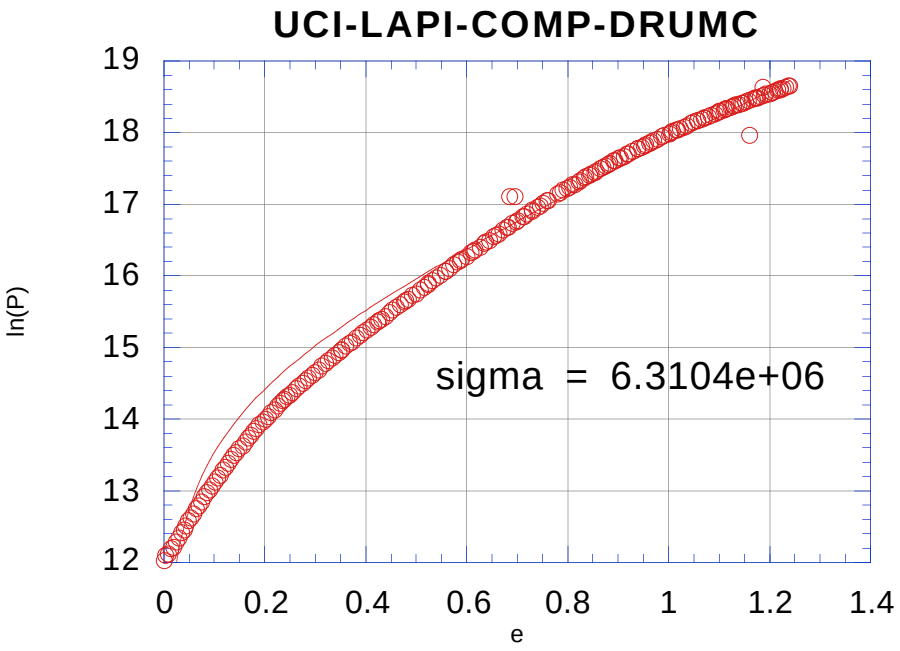
UCI-LAPI-COMP-DRUMC
ln(P)
19
18
17
16
15
14
13
12
0
0.2
0.4
0.6
0.8
1
1.2
1.4
e
sigma = 6.3104e+06

18 c

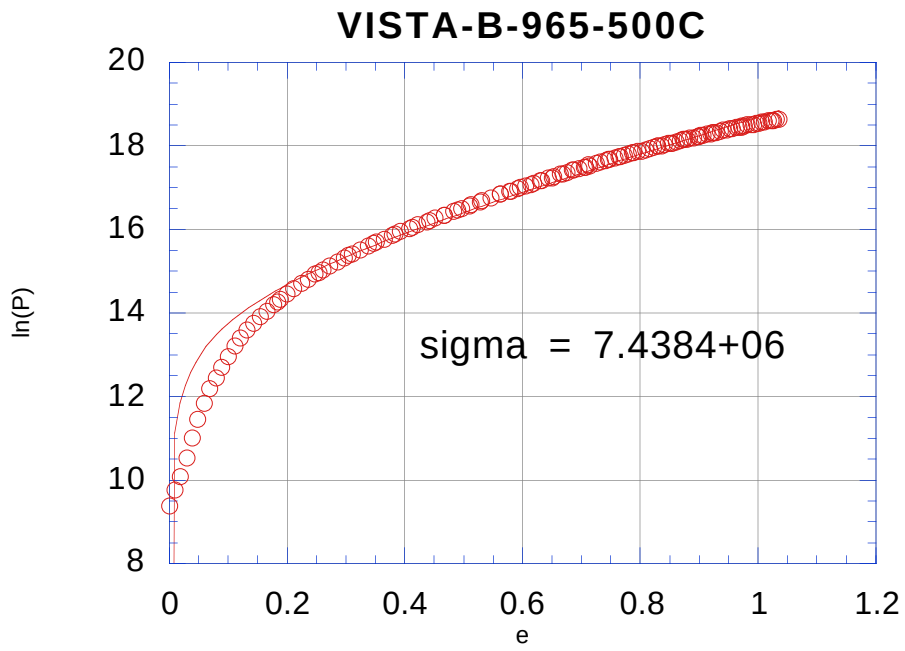
VISTA-B-965-500C
ln(P)
20
18
16
14
12
10
8
0
0.2
0.4
0.6
0.8
1
1.2
e
sigma = 7.4384+06

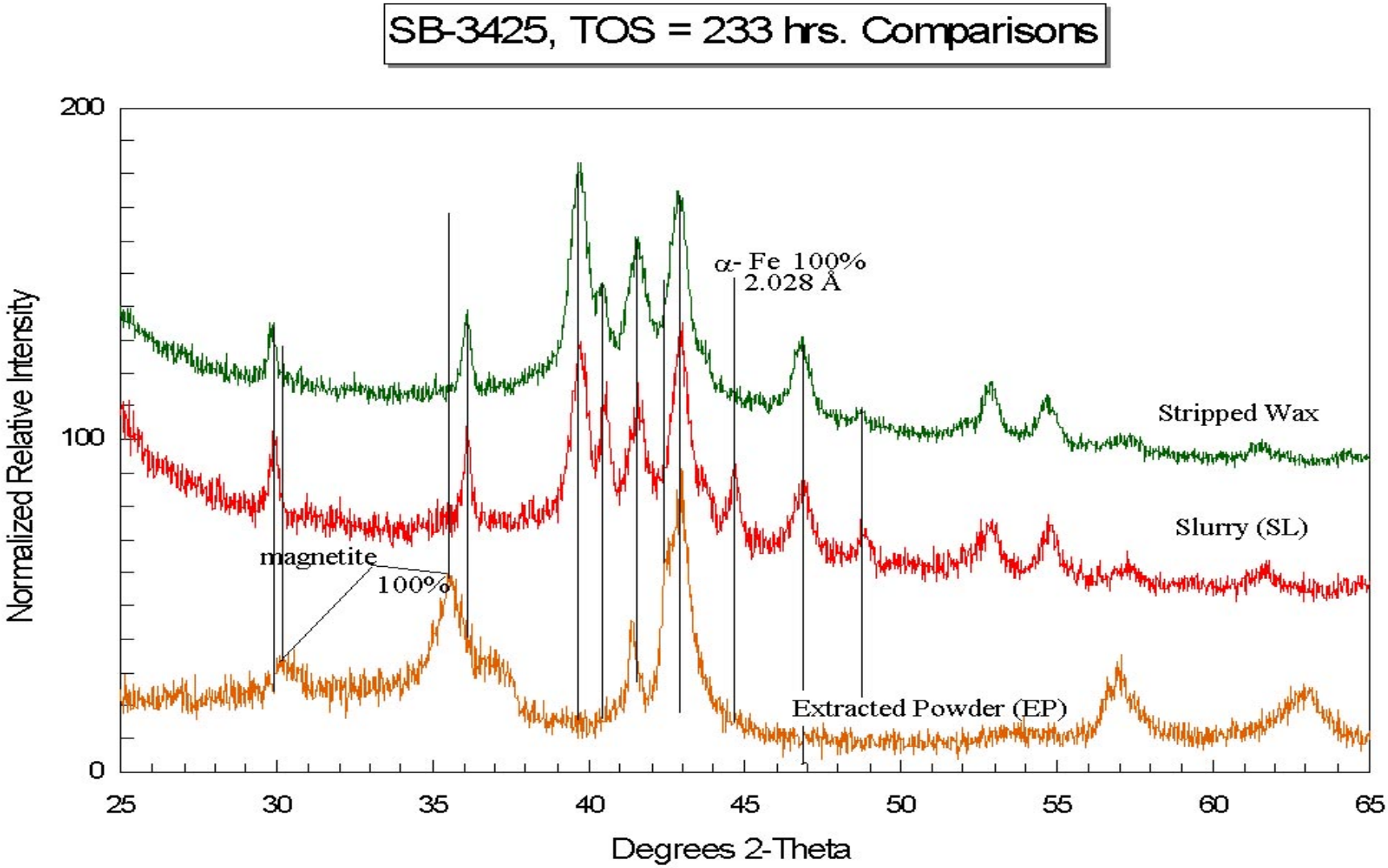

Figure 19 X-ray diffraction powder patterns of the Texas A&M catalyst as-received in the wax (slurry). Also shown is a powder pattern of this catalyst after the wax was extracted via solvent extraction. The pattern at the top comes from the wax alone, free of any catalyst. Note how the α-Fe peak in the as-received catalyst is absent in the solvent extracted sample as well as the wax (which does not contain any catalyst). The magnetite peaks in the solvent extracted sample arise due to sample oxidation and were not seen in the as-rceived sample.

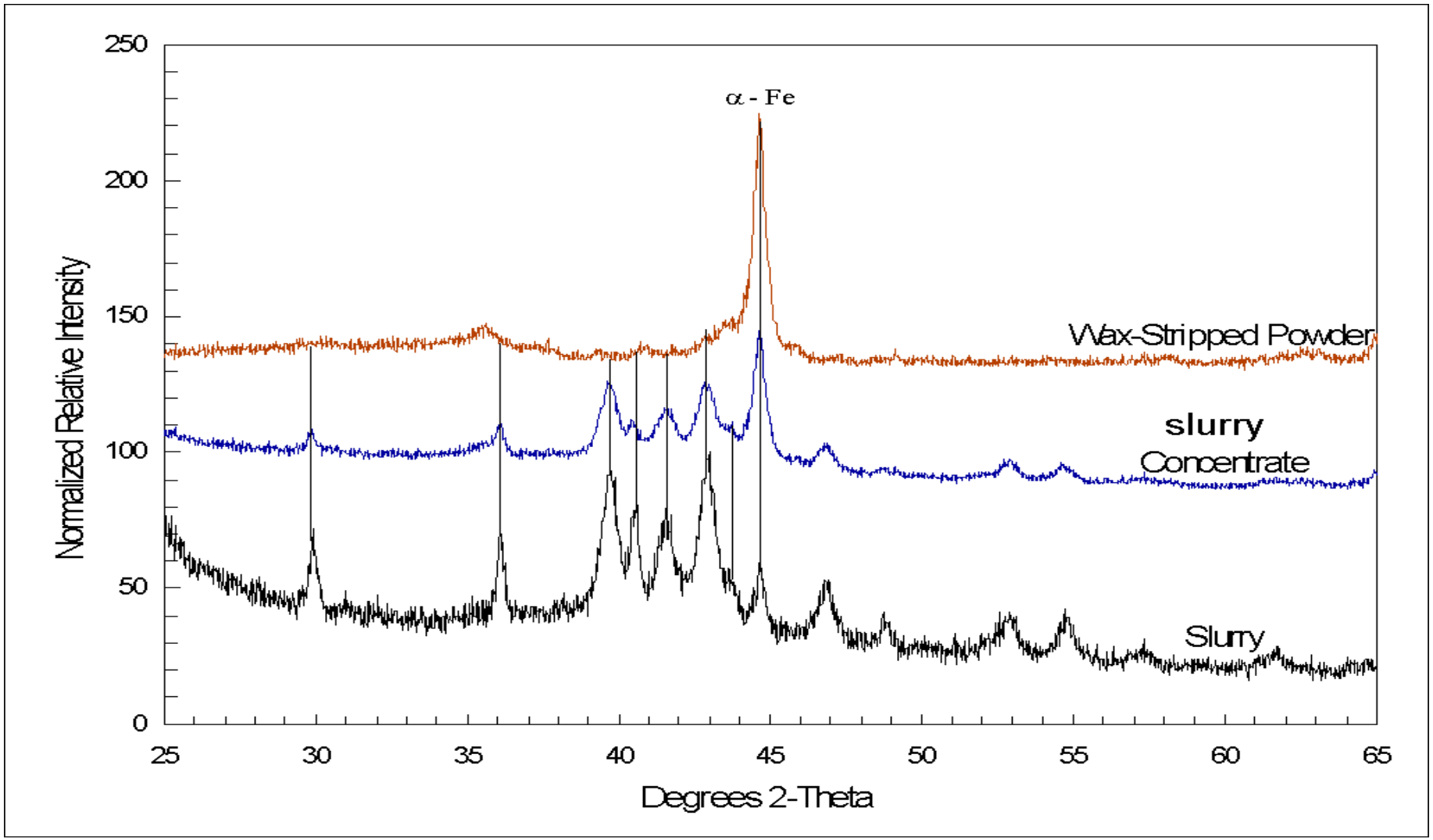

Figure 20 X-ray diffraction powder pattern of the Texas A&M catalyst as -received in wax (slurry). The catalyst loading was increased by allowing it to settle and analyzing the sediment (slurry concentrate). To eliminate peaks from the wax, this concentrate sample was heated in flowing Helium up to 400 °C to strip the wax (wax-stripped powder). The unmistakable conclusion from this series of xrd patterns is that a-Fe is a major constituent of the working catalyst this reactor (run SB-3425 time on stream 330 hours).

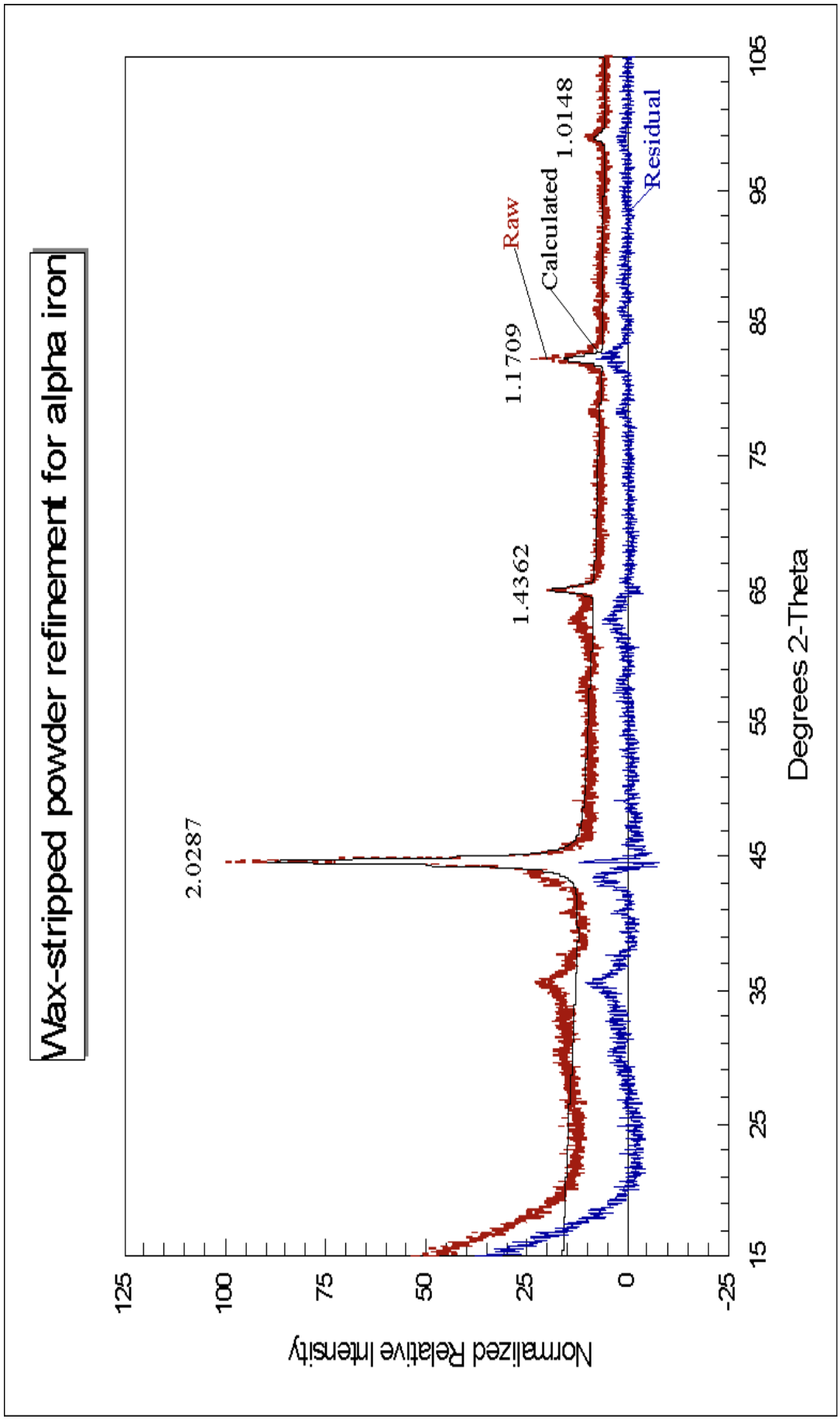

Fig. 21 Reitveld refinement of the xrd pattern of the wax stripped powder shown in Fig. 20. After subtraction of the α-Fe peak, we see some residual peaks that are shown in greater detail in the next figure. The major constituent is definitely α-Fe.

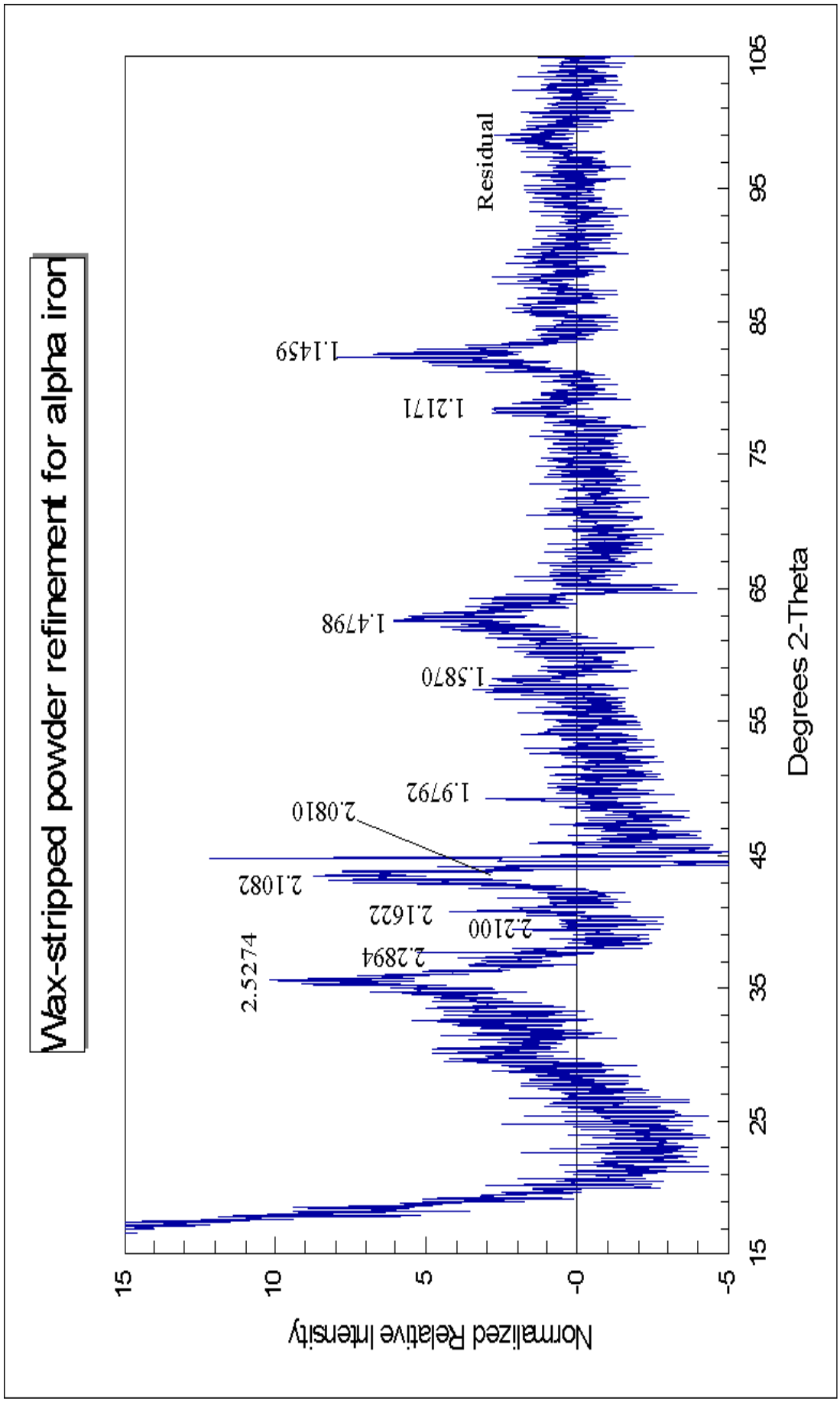

Fig. 22 The residual after subtraction of the α-Fe from the wax-stripped powder. The peak at 2.52 Å may correspond to magnetite while the other peaks may come from iron carbides.

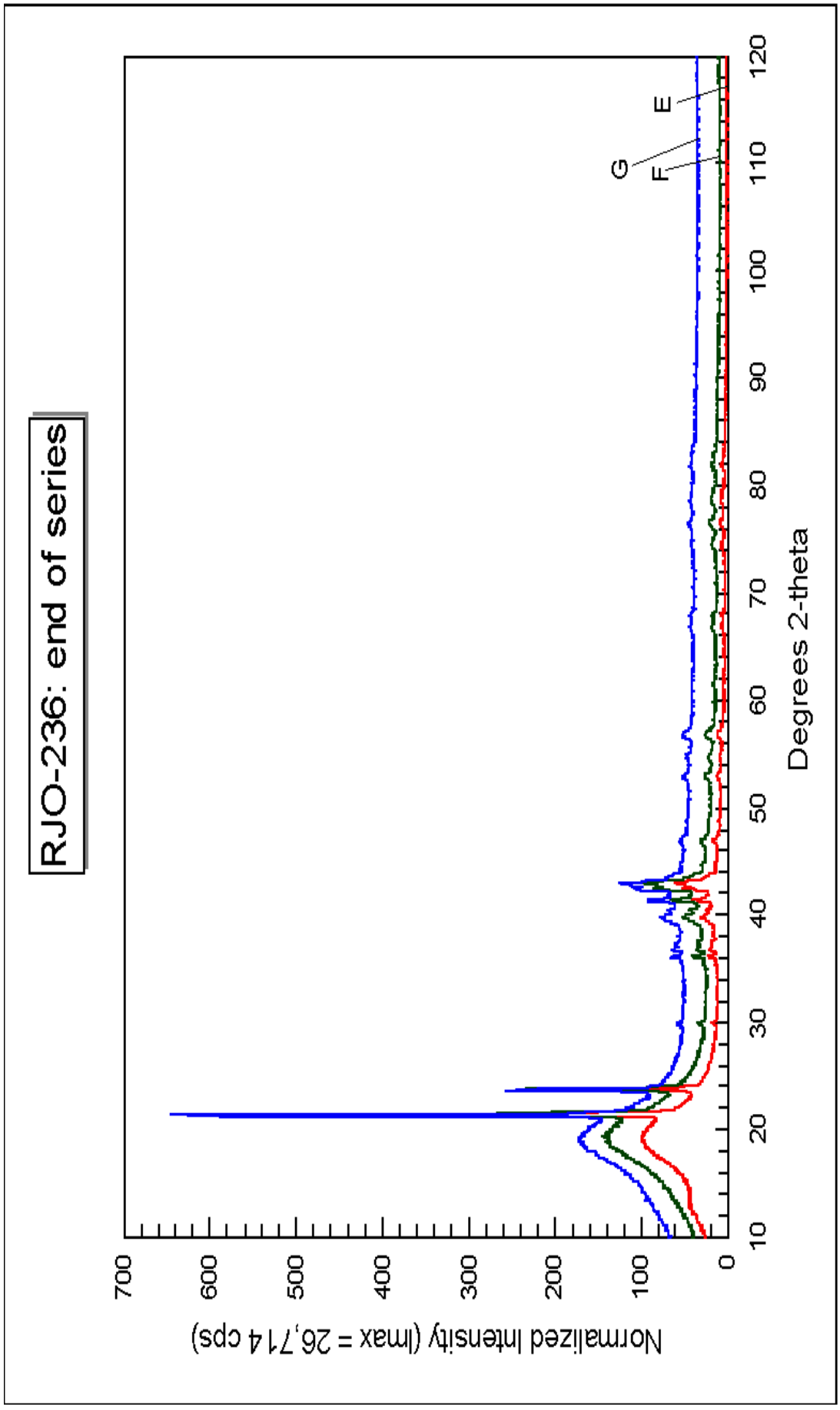

Fig. 23 X-ray diffraction pattern of samples received from CAER from a F-T run. This sample was received in the wax and had been removed under an inert blanket. An expanded view of this xrd pattern is shown in the next figure. Samples E, F and G were withdrawn at increasing time on stream during a F-T run.

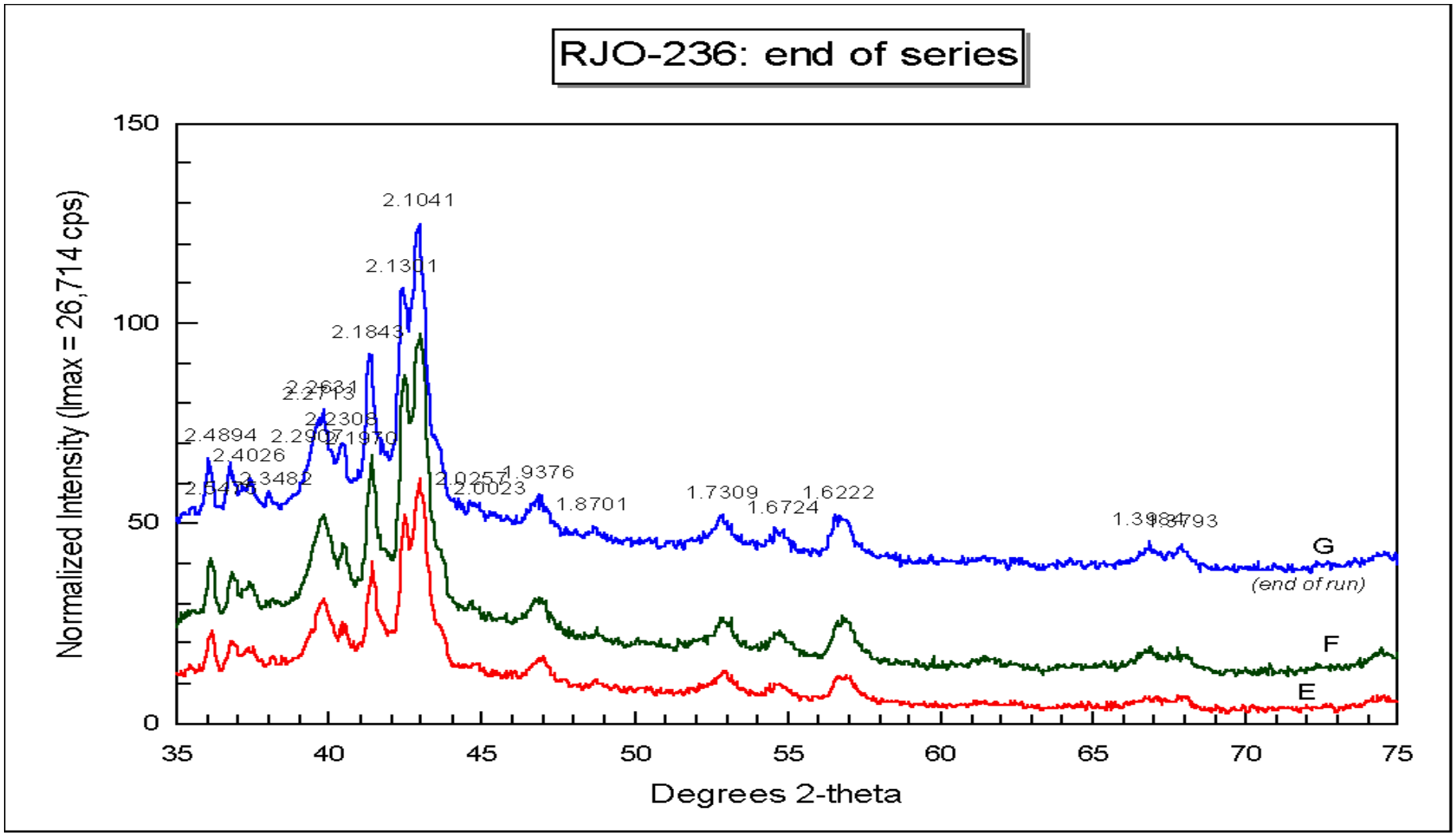

Fig. 24 An expanded view of the xrd patterns shown in Fig. 23. The peaks appear to come from iron carbide and there is no evidence for any magnetite. This result suggests that magnetite may not be present in significant amounts in an F-T slurry reactor. Removal of hot wax under inert blanket is necessary to preserve the phase composition of the working catalyst.